JOURNAL OF PETROLOGY | VOLUME 47 | NUMBER 5 | PAGES 965–990 | 2006 | doi:10.1093/petrology/egi102

Ca-rich Garnet–Clinopyroxene Rocks at Hujialin in the Su–Lu Terrane (Eastern China): Deeply Subducted Arc Cumulates?

JIAN-JUN YANG[1,2]*

[1]STATE KEY LABORATORY OF LITHOSPHERIC EVOLUTION, INSTITUTE OF GEOLOGY AND GEOPHYSICS, CHINESE ACADEMY OF SCIENCES, P.O. BOX 9825, BEITUCHENG XILU 19, BEIJING 100029, P.R. CHINA

[2]THE KEY LABORATORY OF CONTINENTAL DYNAMICS, DEPARTMENT OF GEOLOGY, NORTHWEST UNIVERSITY, XI'AN 710069, P.R. CHINA

RECEIVED APRIL 1, 2005; ACCEPTED DECEMBER 28, 2005
ADVANCE ACCESS PUBLICATION FEBRUARY 13, 2006

*Layers of Ca-rich garnet–clinopyroxene rocks enclosed in a serpentinite body at Hujialin, in the Su–Lu terrane of eastern China, preserve igneous textures, relict spinel in garnet, and exsolution lamellae of Ca-rich garnet, ilmenite/magnetite, Fe-rich spinel, and also amphibole in clinopyroxene. In terms of their major and trace element compositions, the studied samples form a trend from arc cumulates towards Fe–Ti gabbros. Reconstructed augite compositions plot on the trend for clinopyroxene in arc cumulates. These data suggest that the rocks crystallized from mantle-derived magmas differentiated to various extents beneath an arc. The Ca-rich garnet + diopside assemblage is inferred to have formed by compressing Ca-rich augite, whereas the relatively Mg-rich cores of garnet porphyroblasts may have formed at the expense of spinel. The protolith cumulates were subducted from near the crust–mantle boundary (*c. *1 GPa) deep into the upper mantle (4·8 ± 0·6 GPa and 750 ± 50°C). Negatively sloped* P–T *paths for the garnet–clinopyroxene rocks and the corollary of corner flow induced subduction of mantle wedge peridotite are not supported by the available data. Cooling with, or without, decompression of the cumulates after the igneous stage probably occurred prior to deep subduction.*

KEY WORDS: *arc cumulates; Ca-rich garnet; garnet–clinopyroxene rocks; Su–Lu terrane; UHP metamorphism*

INTRODUCTION

Very high-pressure Ca-rich garnet–clinopyroxene rocks including garnetites have been found as layers in ultrahigh-pressure (UHP) metamorphic belts (Evans *et al.*, 1979; Yang, 1991; Becker & Altherr, 1992; Klemd *et al.*, 1994; Becker, 1996; Vrána & Frýda, 2003; Yang *et al.*, 2005) and xenoliths in kimberlites (O'Hara & Mercy, 1966; Harte & Gurney, 1975; Jerde *et al.*, 1993). Whereas some of those associated with marbles and gneisses may be derived from sedimentary protoliths (Becker & Altherr, 1992; Klemd *et al.*, 1994), and some were derived from rodingites (Evans *et al.*, 1979), the origin and cause of the Ca-rich characteristic of others remain unclear. Study of the nature of the protolith and the metamorphic histories of such rocks is important to understand the previous architecture and evolution of orogenic belts, and may shed some light on the origin of xenoliths in kimberlites.

Mineral assemblages of garnet + clinopyroxene ± ilmenite ± magnetite ± Fe-rich spinel/hercynite ± olivine ± amphibole [hereafter Grt–Cpx rocks; mineral abbreviations after Kretz (1983)], with grossular contents in garnet ranging from 36 to 70 mol %, occur as layers in a large serpentinite body at Hujialin, Rizhao County, in the middle of the Su–Lu UHP metamorphic terrane, eastern China (Fig. 1). They were previously named 'garnet clinopyroxenites' and their origin has been the subject of a number of studies. Based on field and petrographical observations, Yang (1991) suggested that they were cumulates in the uppermost mantle, an interpretation supported by the analysis of geochemical data (Jahn, 1999). On the other hand, Zhang *et al.* (1994) considered these rocks to be the 'best relics' of the low-*P* (*P*, pressure; *T*, temperature) protolith of the

*Present address: State Key Laboratory of Lithospheric Evolution, Institute of Geology and Geophysics, Chinese Academy of Sciences, P.O. Box 9825, Beitucheng Xilu 19, Beijing 100029, P.R. China. Telephone: 86-10-62007827. Fax: 86-10-62010846. E-mail: jjyang@mail.igcas.ac.cn

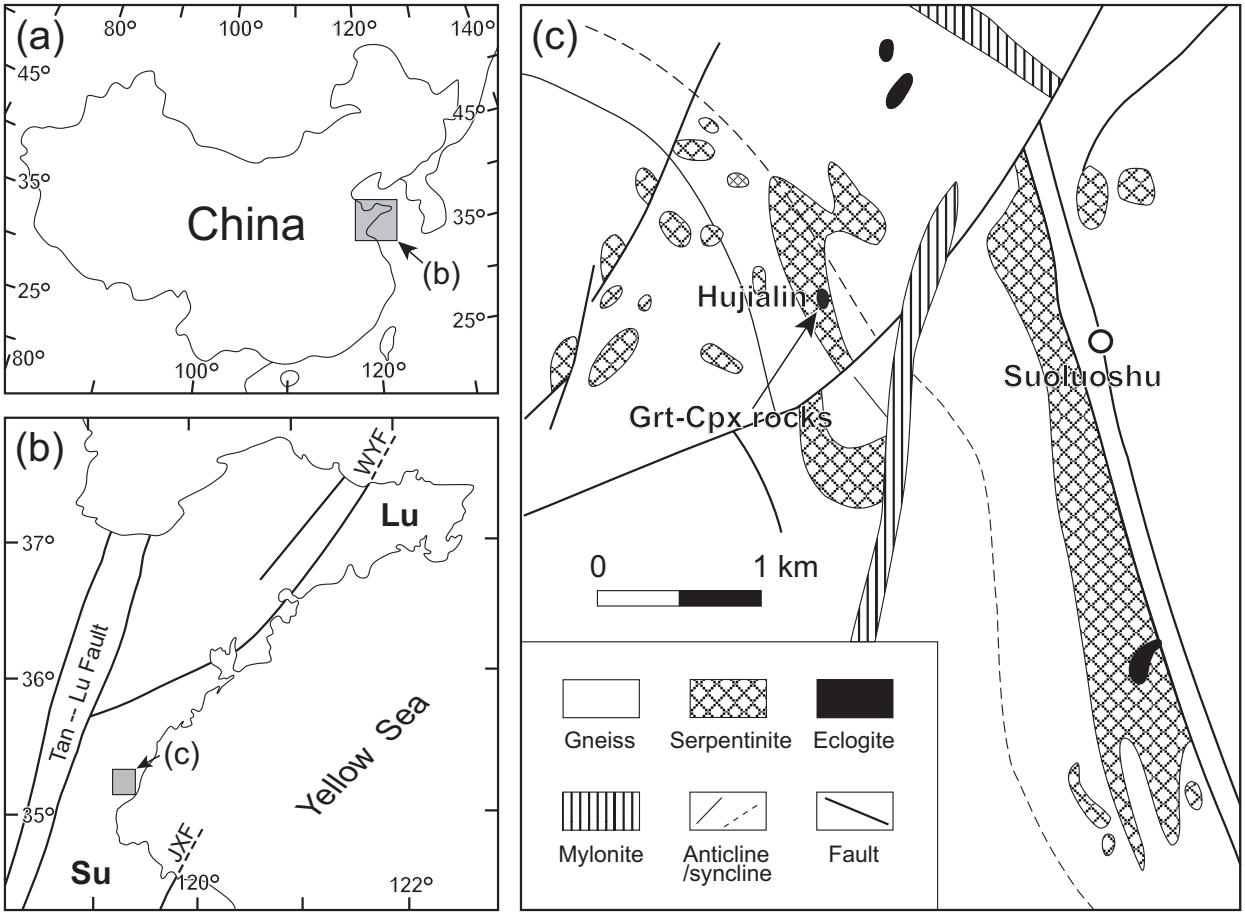

Fig. 1. Simplified geological map of southern Rizhao County. (a) Location of the Su–Lu region (shaded area) in China. (b) Tectonic map of the Su–Lu terrane. Su and Lu are the Chinese abbreviations of Jiangsu and Shandong provinces, respectively. Here they refer to the ultrahigh-pressure metamorphic belt in this region. Shaded area is the location of Hujialin Grt–Cpx and associated ultramafic rocks; JXF, Jiashan–Xiangshui fault; WYF, Wulian–Yantai fault. (c) The field occurrence of the Hujialin Grt–Cpx rocks (indicated by an arrow).

mantle-derived garnet peridotites in the Su–Lu terrane. An early stage of cooling and compression from low-P/high-T to high-P/low-T conditions was proposed by Zhang *et al.* (1994, 2000), based on their P–T estimates for the early stage metamorphism of the Hujialin Grt–Cpx rocks and the peak metamorphic conditions of garnet peridotites from the same terrane. Zhang *et al.* (2000) further argued that garnet peridotites in this region were formerly mantle wedge materials, incorporated into the orogenic belt as a result of corner flow in the wedge. Hiramatsu & Hirajima (1995) proposed a similar P–T path based on a petrological study of the Hujialin Grt–Cpx rocks alone. Most recently, Zhang & Liou (2003) proposed that the Hujialin Grt–Cpx rocks either were derived from clinopyroxenites at 4–5 GPa and 1400°C, which were then subducted to 5–7 GPa and 1000°C, or they might have been formed at >15 GPa and 1500°C. Additionally, the Ca-rich Hujialin Grt–Cpx rocks might also be considered genetically related to seafloor alteration of a mafic protolith, because their CaO contents are higher than the lower CaO limit (15 wt %) for rodingites (Evans *et al.*, 1979).

The present study aims to: (1) investigate the origin and tectonic setting of the protoliths of the Hujialin Grt–Cpx rocks, based on field relations, petrology, whole-rock and mineral major and trace element geochemistry, and isotope data on whole-rocks and minerals; (2) show that UHP metamorphism of spinel clinopyroxenites can produce the Ca-rich Grt–Cpx rocks; (3) evaluate peak metamorphic P–T conditions and discuss the P–T path followed by the Hujialin rocks and its tectonic implications for the Su–Lu–Dabie orogenic belt.

GEOLOGICAL SETTING AND FIELD RELATIONS

The Su–Lu UHP metamorphic region, initially referred to as the 'Su–Lu Coesite–Eclogite Province' by Yang & Smith (1989), is the eastern part of the Triassic Qinling–Dabie–Su–Lu collision belt between the Sino-Korean

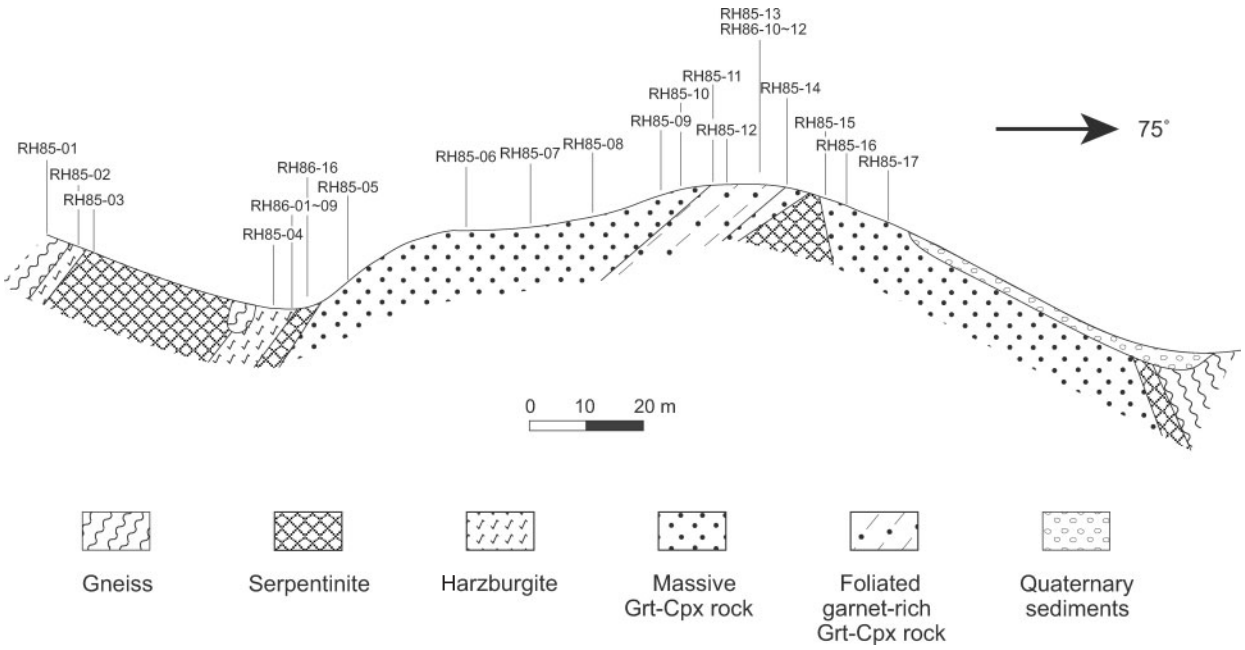

Fig. 2. Geological cross-section through the Hujialin ultramafic complex [modified after Yang (1991)]. The numbers indicate sample locations. All the samples with labels containing 'RH86' and the sample RH85-16 are loose boulders. Rock foliations are shown by the patterned fills.

and Yangtze cratons, offset to the NE from the Dabie terrane by the Tan-Lu fault zone (Fig. 1) (Yang, 1991). It is bounded by the Wulian–Yantai fault to the north and the Jiashan–Xiangshui fault to the south. The Su–Lu terrane, largely corresponding to the 'Jiaonan Group' in old Chinese geological literature, mainly consists of quartzofeldspathic gneisses, migmatites and granitoids, with minor, but widespread, UHP eclogites, amphibolites, metasediments (marbles, jadeite quartzites, etc.) and ultramafic rocks (serpentinites and peridotites). Some eclogites appear within or closely associated with ultramafic rocks, and some are intercalated with country-rock gneisses and metasediments. Sm–Nd and U–Pb dating of the eclogites (Li, 1993; Hacker *et al.*, 1998), UHP gneisses (Liu *et al.*, 2004), and garnet peridotites (Yang & Jahn, 2000) shows that they were all subjected to UHP metamorphism at 245–220 Ma. A parallel blueschist belt occurs to the south of the UHP metamorphic belt.

Numerous serpentinite and eclogite bodies occur within gneiss along folds, faults, and mylonite zones in the SE of Rizhao County (Fig. 1). Several eclogite (with or without quartz/coesite) layers were observed within the largest serpentinite body in this area (Yang, 1991). A serpentinite body occurs at Hujialin in the axis of a synform and is itself folded. Layers of Grt–Cpx rocks are found within the serpentinite.

The Grt–Cpx rock layers are elongated in the south–north direction for *c.* 225 m and together occupy *c.* 105 m in the east–west direction. They display sharp contacts with the enclosing serpentinite. In some drill-core samples they are sandwiched between harzburgite layers and separated from them by a thin layer of a Tlc + Srp + Cal assemblage. A cross-section made along early exploratory trenches dug parallel to the short axis of the Hujialin complex (Yang, 1991) is shown in Fig. 2. The Grt–Cpx rocks are generally massive. Foliated garnet-rich rocks (over 40 vol. % Grt) occur in the central part of the complex. Black boulders of coarse-grained augite with garnet lamellae are found near the central part of the body. Their original contact relationship with other Grt–Cpx rocks, however, is not exposed. The Grt–Cpx rock layers split along the long axis into thin veins and merge into the serpentinite at the northern boundary of the outcrop (Fig. 3a). In places, garnet-rich and diopside-rich bands are strongly folded. Garnet locally concentrates to form garnetite (Fig. 3b). Magnetite veins (0·5–1·0 cm wide) are observed in the Grt–Cpx rock layers. Garnet-poor and diopside-rich rocks appear in the outer parts of the body. Sensitive high-resolution ion microprobe (SHRIMP) dating of zircon grains separated from some olivine-bearing Grt–Cpx rocks gave ages ranging from 223·1 ± 8·4 Ma to 185·2 ± 7·4 Ma (Gao *et al.*, 2004), which were interpreted to represent the age of exhumation.

Blocks of harzburgite occur in the SW of the Grt–Cpx rock complex (Fig. 2). The harzburgite is fine-grained, massive, and fresh, and is clearly distinguishable from

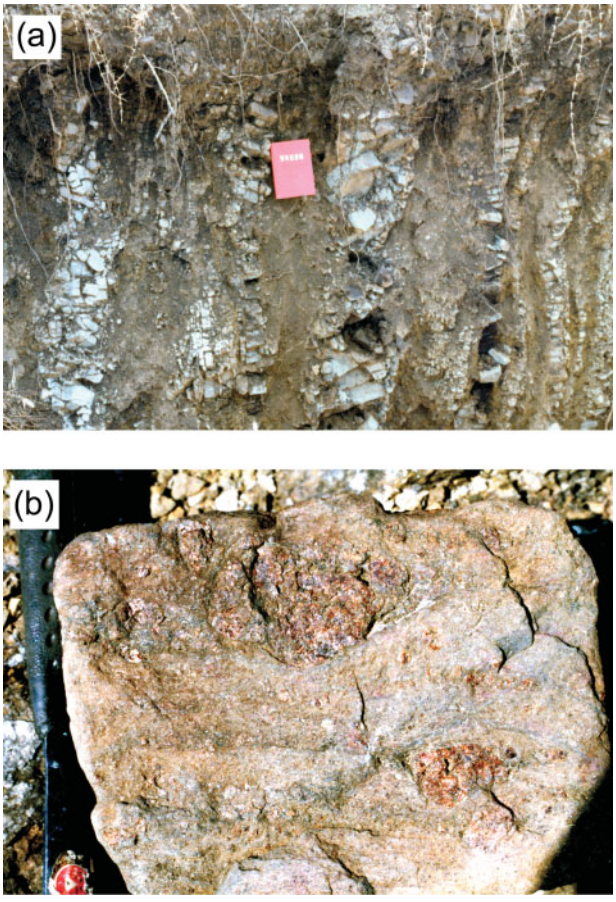

Fig. 3. Field views of the Hujialin complex. (a) Interbanded Grt–Cpx rocks (protruding bands) and serpentinite (recessed bands); (b) garnet-rich aggregates.

the strongly weathered enclosing serpentinite. The harzburgite and the host serpentinite display sharp contacts. The gneiss is strongly foliated near the boundary with serpentinite.

PETROGRAPHY

Grt–Cpx rocks

Clinopyroxene and garnet are predominant in the rocks. Based on texture and modal abundance, four types of Grt–Cpx rocks are distinguished.

Type I is represented by the black boulders (RH86-10 to RH86-12) (up to 20 cm) and is dominated by coarse-grained (up to 6 mm) augite. The grain boundaries suggest an igneous texture (Fig. 4a). Extensive exsolution lamellae (up to 3 mm long) of garnet, opaque minerals, and green spinel occur inside and at the boundaries of the augite. The opaque mineral lamellae are often armoured by garnet (Fig. 4b). Large augite grains also include coarse opaque minerals, and in some cases, amphibole (Fig. 4c). Fine amphibole lamellae are seen in the same augite grain when viewed as a backscattered electron (BSE) image (Fig. 4d), occupying *c.* 14 vol. % of the whole image. In places, green spinel tablets appear as the only exsolved mineral. Local deformation has caused undulose extinction in augite containing broken lamellae and fine grains (0·02–0·07 mm) of garnet, green spinel, and residual diopside.

Type II Grt–Cpx rock is the most abundant and is composed of porphyroblasts (up to *c.* 3 mm) of pinkish yellow garnet in a matrix of fine-grained (up to *c.* 0·7 mm) pale green diopside, opaque minerals associated with green spinel, and yellow garnet (Fig. 4e). Aligned garnet porphyroblasts form bands; they include rounded clinopyroxene, opaque minerals, and/or spinel grains. In some cases, the clinopyroxene inclusions in turn enclose garnet and/or opaque lamellae. Small garnet grains cluster in groups and form up to 40 vol. % of the matrix. Aggregates of magnetite and spinel are abundant in some samples. In rare cases, some large augite grains appear to be xenocrysts with lamellar or rounded garnet and magnetite inclusions. They are interpreted as relict augite from type I Grt–Cpx rocks.

Type III Grt–Cpx rock is garnetite; these are boulders dominated by variable sized garnet (Fig. 3b). They can be further divided into three subtypes. One of these (RH85-16) consists of aggregates of small (*c.* 0·1 mm) garnet grains, which look like large poikiloblastic garnet crystals (up to 10 cm) in hand specimen. Minor amounts of diopside and opaque minerals occur as inclusions or interstitial grains between the small garnet grains. BSE imaging shows that some magnetite grains contain oriented ilmenite lamellae in this sample. Another subtype (RH86-01) consists of large garnet grains (up to 4 mm), replaced by epidote, amphibole, and titanite. The garnet is free of clinopyroxene inclusions but contains acicular needles of rutile (Fig. 4g), which display inclined extinction under cross-polarized light. A third subtype (RH86-16) consists of garnet megacrysts (up to 1·5 cm) including rounded grains of clinopyroxene (1–3 mm), which contain extremely narrow plates of opaque minerals, larger ilmenite inclusions with magnetite and hercynite lamellae, and, rarely, *c.* 0·15 mm garnet lamellae (Fig. 4h). This megacrystic garnet does not contain rutile needles.

Type IV Grt–Cpx rock is diopsidite consisting mainly of fine-grained diopside (Fig. 3a), with minor garnet and olivine.

Ultramafic rocks (serpentinite and harzburgite)

Massive serpentinite samples are mainly composed of serpentine, chlorite, and magnetite. Foliated harzburgite contains rare orthopyroxene and amphibole porphyroblasts (up to *c.* 2 mm) set in a fine-grained (up to *c.* 0·7 mm)

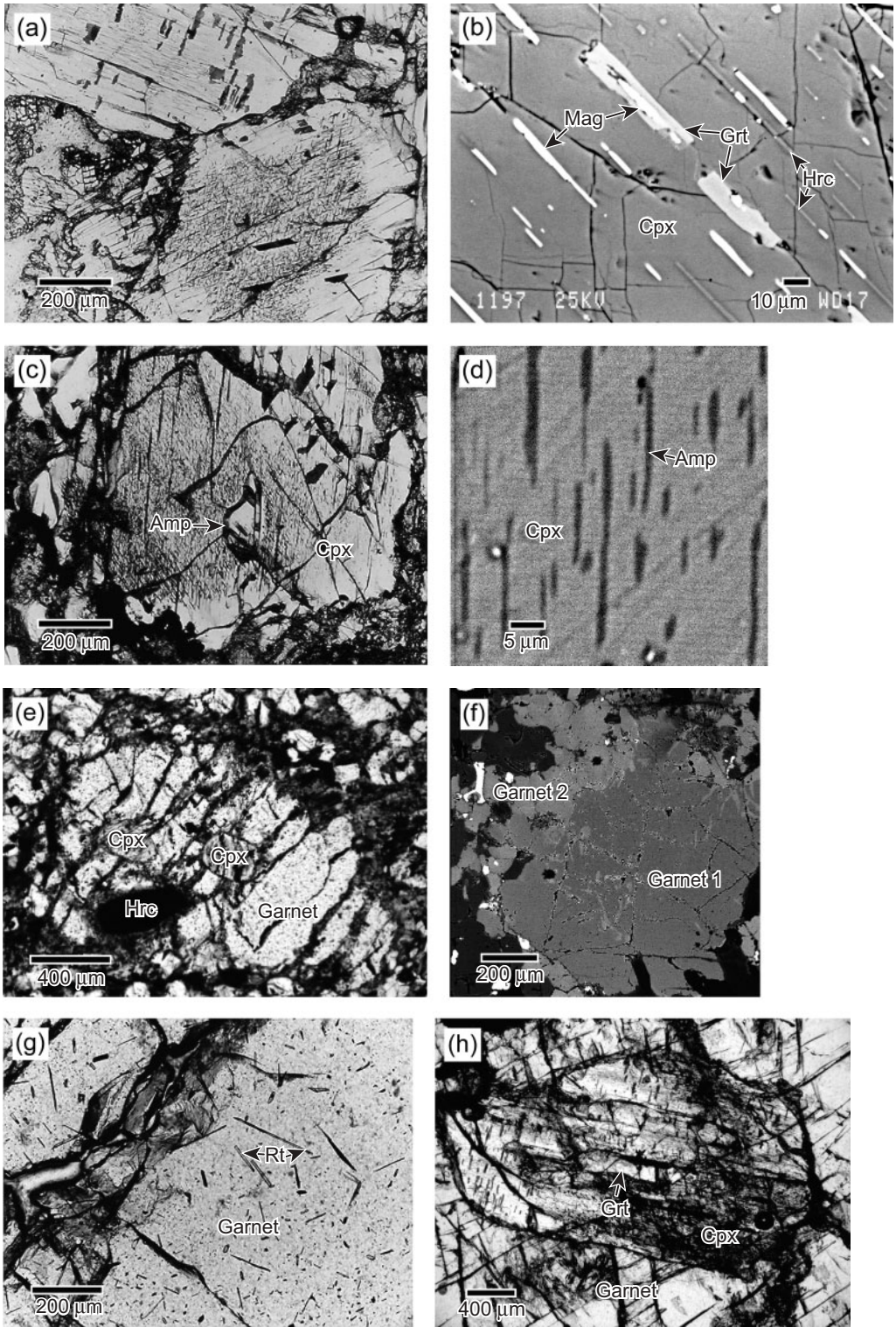

Fig. 4. Photomicrographs (all under plane-polarized light) and backscattered electron (BSE) images of the Grt–Cpx rocks. (a) Igneous texture of clinopyroxenite (RH85-08); (b) BSE image of augite with garnet, magnetite, and hercynite exsolution lamellae (RH86-12); (c) amphibole inclusion in augite (RH85-08); (d) BSE image of amphibole lamellae in the same augite crystal as shown in (c); (e) porphyroblastic texture of the most abundant type II Grt–Cpx rock (RH85-13); (f) BSE image of porphyroblastic garnet (RH86-06); the garnet core (Garnet 1) and the more Ca-rich garnet rim (Garnet 2) are in sharp contact; (g) rutile needles in coarse-grained garnet (RH86-01); (h) clinopyroxene with garnet lamellae is included in megacrystic garnet (RH86-16).

Table 1: Whole-rock major element compositions

Rock type:	Garnet–clinopyroxene rocks									Harzburgite	Serpentinite	
Subtype:	IV	II	II	II	II	II	II	II	I			
Sample:	RH85-05	RH85-11	RH85-12	RH85-13	RH85-17	RH86-04*	RH86-05*	RH86-06*	RH86-10*	RH85-04b	RH85-701	RH85-702b
SiO_2	47·59	47·79	47·63	37·59	46·01	36·55	33·55	44·24	36·10	43·01	40·56	38·66
TiO_2	0·62	1·88	1·17	4·24	1·38	4·36	5·16	1·35	5·02	0·03	0·03	0·04
Al_2O_3	3·15	4·68	6·47	6·40	5·59	10·75	9·53	12·38	7·01	0·51	1·63	1·33
Fe_2O_3	7·43	8·74	7·31	21·06	8·90	10·33	13·15	3·96	12·89	8·17	5·74	7·01
FeO						8·77	11·10	4·85	9·05			
MnO	0·09	0·11	0·09	0·16	0·10	0·19	0·18	0·15	0·15	0·11	0·09	0·11
MgO	21·59	15·39	15·79	11·65	16·61	11·39	11·49	14·38	11·45	44·57	38·44	38·11
CaO	16·18	19·15	20·00	18·03	17·91	17·06	15·86	18·10	17·32	0·27	0·03	0·52
Na_2O	0·32	0·61	0·41	0·36	0·57	0·28	0·16	0·32	0·20	0·08	0·03	0·05
K_2O	0·02	0·14	0·04	0·01	0·13	0·08	0·03	0·02	0·01	0·03	0·11	0·03
P_2O_5	0·01	0·01	0·01	0·01	0·01	0·01	0·01	0·02	0·01	0·01	0·01	0·01
LOI	2·63	1·10	0·60	0·00	2·54					3·12	13·31	14·3
Total	99·63	99·60	99·52	99·51	99·75	99·77	100·22	99·77	99·21	99·91	99·98	100·17
100Mg/(Mg + Fe)	85·20	77·73	81·06	52·30	78·72	52·92	47·18	75·29	49·72	91·53	92·99	91·51
100Cr/(Cr + Al)	6·74	3·24	2·73	0·07	1·76					32·65	15·32	16·92

*Data from Yang (1991).

matrix of olivine, orthopyroxene, talc, amphibole, chromite, and chlorite. Orthopyroxene is surrounded by talc and olivine. Orthopyroxene and chromite also appear as separate inclusions in olivine. Fine chromite grains, some with rims altered into spinel, form elongated aggregates in the matrix.

ANALYTICAL METHODS

Whole-rock major and trace element analysis

The major element compositions of representative samples were analysed by X-ray fluorescence (XRF; Rigaku 2100) and trace elements by solution inductively coupled plasma mass spectrometry (ICP-MS; Elan 6100DRC), at The Key Laboratory of Continental Dynamics (KLCD), Northwest University (Xi'an). A dissolution bomb was heated to 190°C for 36 h to guarantee complete dissolution of refractory accessory minerals such as zircon. FeO was analysed by the conventional titrimetic method. The difference between total FeO and FeO was then converted into Fe_2O_3. The analytical uncertainties (2σ) are: <1% for SiO_2, Fe_2O_3 and MgO; <5% for Al_2O_3, CaO and MnO; <10% for Na_2O and K_2O; and 10% to 20% for TiO_2 and P_2O_5, respectively. For trace elements, the uncertainties vary from <5% to <20%, depending on the concentration levels. The fine-grained garnetites (type III Grt–Cpx rocks) consisting of >90 vol. % garnet were not analysed. The data are listed in Tables 1 and 2.

Mineral major and trace element analysis

Major elements in minerals were analysed using a wavelength-dispersive electron microprobe (Cameca SX51) at the Institute of Geology and Geophysics, Chinese Academy of Sciences (Beijing). Analytical conditions were accelerating voltage 15 kV, beam current 20 nA, electron beam diameter 1 μm, and counting time 10 s, except for P, which was counted for 20 s. P was analysed only in a garnet sample containing an appreciable amount of Na (Table 3). The program PAP provided by Cameca was used for matrix corrections. Mineral formulae, including Fe^{3+}/Fe^{2+}, were calculated by assuming stoichiometry and charge balance (Droop, 1987). Mineral end-members were calculated following Yang (1992). Representative data are given in Tables 3–6.

Trace elements in a coarse clinopyroxene grain with less extensive exsolution of garnet and ilmenite, a clinopyroxene inclusion and the host garnet, were analysed at KLCD by ICP-MS (Elan 6100DRC) coupled with a 193 nm ArF-excimer Laser (ComPex 102) ablation system (GeoLas 200 M) (ELA-ICP-MS). Maximum beam energy was 210 mJ and spot size was 60 μm. Helium was used as the carrier gas. The external standard was NIST610. Given the interference of ^{43}Ca by $^{27}Al^{16}O$,

Table 2: Whole-rock trace element abundances

Rock type:	Garnet–clinopyroxene rocks					Harzburgite	Serpentinite	
Sample:	RH85-05	RH85-11	RH85-12	RH85-13	RH85-17	RH85-04b	RH85-701	RH85-702b
La	1·73	2·42	1·67	2·52	1·32	0·09	0·87	0·54
Ce	5·63	8·51	5·96	10·36	5·44	0·12	2·05	1·20
Pr	1·04	1·66	1·10	2·25	1·09	0·02	0·26	0·16
Nd	5·84	10·3	6·72	15·4	6·91	0·09	1·08	0·73
Sm	1·52	2·98	2·03	4·36	2·04	0·02	0·25	0·14
Eu	0·45	0·88	0·73	1·28	0·70	0·01	0·012	0·053
Gd	1·34	2·73	1·98	4·05	1·96	0·02	0·24	0·14
Tb	0·201	0·436	0·315	0·620	0·308	0·004	0·036	0·016
Dy	0·96	2·06	1·57	2·91	1·55	0·02	0·25	0·13
Ho	0·163	0·337	0·270	0·467	0·256	0·004	0·051	0·023
Er	0·39	0·76	0·60	1·03	0·56	0·02	0·15	0·077
Tm	0·047	0·086	0·067	0·11	0·061	0·002	0·019	0·005
Yb	0·29	0·51	0·43	0·63	0·38	0·015	0·17	0·09
Lu	0·038	0·070	0·055	0·085	0·049	0·003	0·019	0·007
Rb	0·53	1·40	1·90	0·88	1·29	0·42	3·26	0·97
Ba	7·00	34·2	49·9	26·1	28·0	9·3	9·93	16·38
Li	2·23	2·45	1·98	2·23	3·68	2·28	34·5	2·97
Be	0·061	0·16	0·075	0·21	0·089	<0·001	0·29	<0·001
Cs	0·060	0·166	0·126	0·078	0·071	0·036	0·188	0·072
Ga	4·11	8·36	8·63	18·5	8·46	0·53	1·75	1·58
Ge	1·51	1·80	1·69	1·79	1·64	0·82	0·94	0·85
Cu	25·2	59·1	39·7	67·7	56·0	4·1	3·50	28·0
Zn	30·1	50·5	34·6	156	42·8	54·8	52·0	46·5
Th	0·078	0·124	0·066	0·080	0·035	<0·01	0·74	0·026
U	0·053	0·030	0·018	0·077	0·024	<0·01	0·128	0·006
Ta	0·028	0·082	0·046	0·059	0·034	0·021	0·053	0·084
Nb	0·12	1·49	0·27	0·20	0·22	0·06	0·55	1·46
Sr	58·3	140	102	112	86·4	2·7	1·77	3·63
Zr	10·9	19·4	17·7	25·8	12·9	0·6	4·95	2·43
Hf	0·63	1·46	1·12	1·92	1·01	0·019	0·20	0·085
Y	3·90	7·92	6·44	11·1	5·93	0·15	1·60	0·87
Sc	54·3	68·0	68·3	51·7	64·2	6·0	10·5	9·7
V	162	229	206	681	221	20	34·2	36·7
Co	62·2	44·5	44·7	72·9	56·3	112·1	122	114
Ni	544	210	296	102·2	315	2072	2357	2371
Cr	2322	1600	1855	48·4	1021	2522	3008	2763

^{42}Ca was used as an internal standard. International standards of fused geological materials BCR-2G, BHVO-1G, AGV-1G, and BIR-1G were directly analysed by ELA-ICP-MS before analysing the samples. The relative analytical uncertainties for the elements vary from <5% to <20%, depending on the concentration levels. More analytical details have been given by Gao *et al.* (2002). The data are listed in Table 7.

WHOLE-ROCK MAJOR AND TRACE ELEMENT COMPOSITIONS

A major characteristic of the Hujialin Grt–Cpx rocks is that they all have high CaO (≥15·86 wt %) and low Na_2O (≤0·61 wt %) contents. MgO is negatively correlated with ΣFeO, Al_2O_3, and TiO_2, and positively correlated with SiO_2 (Fig. 5). Zr and V are negatively

Table 3: Selected electron microprobe analyses of ilmenite and garnet

Rock type:	Garnet–clinopyroxene rocks														Garnetite	
Mineral:	Ilmenite				Garnet											
Sample:	RH86-06	RH86-06	RH85-13	RH86-03	RH86-12	RH86-12	RH86-12	RH86-12	RH86-01	RH86-01	RH86-06	RH86-06	RH85-08	RH85-08	RH86-16	RH85-16
Position:	Grain in matrix		In Grt	Lam in Cpx	Lam-rim1	Lam-core1	Lam-rim2	Lam-core2	Large garnet*	σ*	Core porph	Fine grain	Core	Rim	Megacryst	Fine grain
SiO_2	0·00	0·22	0·06	0·10	40·33	39·81	40·21	39·53	40·04	0·135	40·94	41·00	39·53	40·01	41·21	39·24
TiO_2	52·23	52·70	51·20	51·33	0·41	0·40	0·36	0·36	0·24	0·050	0·16	0·10	0·38	0·32	0·13	0·21
Al_2O_3	0·00	0·12	0·07	0·00	20·04	21·40	21·48	21·46	22·29	0·052	22·53	20·55	20·80	20·46	22·38	20·84
Cr_2O_3	0·22	0·13	0·00	0·00	0·00	0·00	0·02	0·14	0·02	0·013	0·10	0·09	0·00	0·09	0·19	0·04
FeO	43·41	43·36	46·32	45·84	8·93	9·92	9·03	10·12	10·06	0·187	9·67	10·30	11·36	9·85	10·40	11·05
MnO	0·48	0·62	1·44	1·37	0·57	0·67	0·55	0·57	0·09	0·042	0·22	0·32	0·75	0·62	0·31	0·15
NiO	0·00	0·31	0·00	0·06	0·00	0·00	0·00	0·00	0·02	0·008	0·00	0·18	0·00	0·00	0·00	0·00
MgO	3·08	3·09	1·30	0·81	7·75	6·37	5·55	5·98	5·95	0·073	10·87	8·13	6·23	4·98	11·35	5·63
CaO					20·65	21·56	23·12	22·05	21·39	0·145	15·58	19·53	21·39	24·16	13·88	22·21
Na_2O					0·08	0·00	0·04	0·04	0·08	0·024	0·02	0·00	0·00	0·02	0·02	0·00
P_2O_5									0·02	0·014						
Total	99·42	100·54	100·40	99·50	98·76	100·13	100·36	100·25	100·18	0·307	100·09	100·20	100·44	100·51	99·88	100·46
O	3	3	3	3	12	12	12	12	12		12	12	12	12	12	12
Si	0·000	0·005	0·002	0·003	3·042	2·982	3·008	2·962	2·995	0·010	3·007	3·053	2·965	3·004	3·035	2·974
Ti	0·973	0·970	0·951	0·972	0·023	0·023	0·020	0·020	0·014	0·003	0·009	0·006	0·021	0·018	0·007	0·012
Al	0·000	0·003	0·002	0·000	1·782	1·890	1·894	1·896	1·965	0·007	1·951	1·804	1·839	1·811	1·943	1·862
Cr	0·004	0·002	0·000	0·000	0·000	0·000	0·001	0·008	0·001	0·001	0·006	0·005	0·000	0·005	0·011	0·002
Fe^{3+}	0·049	0·043	0·089	0·050	0·097	0·101	0·055	0·137	0·028	0·021	0·014	0·074	0·188	0·142	0·000	0·162
Fe^{2+}	0·850	0·844	0·868	0·915	0·468	0·524	0·511	0·501	0·602	0·017	0·581	0·570	0·530	0·480	0·639	0·543
Mn	0·010	0·013	0·030	0·029	0·036	0·043	0·035	0·036	0·006	0·003	0·014	0·020	0·048	0·039	0·020	0·010
Ni	0·000	0·006	0·000	0·001	0·000	0·000	0·000	0·000	0·000	0·000	0·000	0·011	0·000	0·000	0·000	0·000
Mg	0·114	0·113	0·048	0·030	0·871	0·711	0·619	0·668	0·664	0·008	1·190	0·902	0·696	0·557	1·245	0·636
Ca					1·669	1·730	1·853	1·770	1·714	0·010	1·226	1·558	1·719	1·944	1·095	1·804
Na					0·012	0·000	0·006	0·006	0·011	0·004	0·003	0·000	0·000	0·003	0·003	0·000
P									0·001	0·001						
Total	2·000	2·000	2·000	2·000	8·002	8·003	8·001	8·004	8·001	0·001	8·000	8·002	8·006	8·004	7·999	8·005

*Average and standard deviation of 16 analyses. Lam: lamellar; porph: porphyroblast.

Table 4: Selected electron microprobe analyses of pyroxenes

Rock type:	Clinopyroxene in garnet–clinopyroxene rocks										Orthopyroxene in harzburgite			
Sample:	RH86-12	RH86-12	RH86-12	RH86-12	RH86-12	RH86-12	RH86-06	RH85-08	RH86-16	RH85-16	RH85-16	RH85-04	RH85-04	RH85-04
Remark:	Rim1-1	Core1	Rim1-2	Rim2-1	Core2	Rim2-2	Host of Ol	Host of Amp	In garnet	In garnet	Matrix	Core	Rim	Small blast
SiO_2	52·14	51·07	52·47	54·41	55·05	54·31	54·29	53·14	53·18	53·70	54·82	59·09	58·59	58·58
TiO_2	0·68	0·56	0·40	0·15	0·07	0·17	0·00	0·16	0·21	0·25	0·04	0·00	0·04	0·03
Al_2O_3	3·74	5·06	3·53	1·55	1·50	2·01	0·61	2·13	2·43	2·04	0·56	0·16	0·32	0·25
Cr_2O_3	0·01	0·15	0·00	0·15	0·00	0·01	0·21	0·02	0·07	0·22	0·10	0·08	0·12	0·06
FeO	3·29	2·90	3·10	2·52	2·09	2·27	1·98	1·93	1·96	3·46	2·25	4·99	5·28	5·35
MnO	0·10	0·08	0·00	0·11	0·01	0·00	0·00	0·00	0·03	0·01	0·05	0·18	0·14	0·22
MgO	15·88	15·54	15·74	17·19	17·01	16·42	16·62	16·24	15·98	15·33	15·99	35·63	34·95	35·86
CaO	24·19	24·12	24·19	24·21	24·28	23·91	24·56	24·08	24·24	24·46	25·28	0·03	0·05	0·07
Na_2O	0·65	0·65	0·60	0·73	0·73	0·70	0·49	0·70	0·57	0·86	0·58	0·01	0·00	0·00
Total	100·68	100·15	100·03	101·02	100·74	99·80	98·77	98·39	98·63	100·32	99·66	100·17	99·49	100·39
O = 6														
Si	1·883	1·851	1·907	1·949	1·976	1·972	1·994	1·954	1·955	1·951	2·002	2·023	2·024	2·001
Ti	0·018	0·015	0·011	0·004	0·002	0·005	0·000	0·004	0·006	0·007	0·001	0·000	0·001	0·001
Al^{IV}	0·117	0·149	0·093	0·051	0·024	0·028	0·006	0·046	0·045	0·049	0·000	0·000	0·000	0·000
Al^{VI}	0·042	0·067	0·058	0·015	0·040	0·058	0·020	0·046	0·060	0·039	0·026	0·030	0·037	0·011
Cr	0·000	0·004	0·000	0·004	0·000	0·000	0·006	0·000	0·001	0·006	0·003	0·002	0·003	0·001
Fe^{3+}	0·082	0·089	0·055	0·074	0·031	0·010	0·016	0·041	0·019	0·050	0·008	0·000	0·000	0·001
Fe^{2+}	0·018	0·000	0·039	0·002	0·032	0·059	0·045	0·019	0·041	0·055	0·060	0·142	0·152	0·152
Mn	0·003	0·002	0·000	0·003	0·000	0·000	0·000	0·000	0·001	0·000	0·001	0·005	0·004	0·006
Mg	0·855	0·839	0·852	0·918	0·910	0·889	0·910	0·890	0·875	0·830	0·870	1·818	1·799	1·825
Ca	0·936	0·937	0·942	0·929	0·934	0·930	0·967	0·949	0·955	0·952	0·989	0·001	0·002	0·002
Na	0·046	0·046	0·042	0·051	0·051	0·049	0·035	0·050	0·041	0·061	0·041	0·001	0·000	0·000
Total	4·001	4·001	4·000	4·000	4·000	4·000	3·999	4·000	4·000	4·000	4·000	3·999	3·999	4·000

Table 5: Selected electron microprobe analyses of spinel group minerals and olivine

Rock type:	Garnet–clinopyroxene rocks								Harzburgite	Grt-Cpx rock		Harzburgite	
Mineral:	Magnetite	Hercynite		Titanian magnetite			Chromian magnetite		Chromite	Ol in Di	Ol in matrix	Ol in matrix	
Sample:	RH86-16	RH86-16	RH86-06	RH86-08	RH86-08	RH86-08	RH85-09	RH85-09	RH85-04	RH86-06	RH86-06	RH85-04	RH85-04
SiO_2	0·01	0·01	0·03	0·21	0·20	0·00	0·16	0·14	0·01	40·94	40·55	41·99	41·82
TiO_2	2·68	1·56	0·06	3·75	5·80	4·75	0·98	2·93	0·29	0·07	0·00	0·09	0·03
Al_2O_3	0·43	58·53	59·72	1·44	2·49	6·37	0·88	0·82	15·87	0·00	0·01	0·00	0·00
Cr_2O_3	1·75	3·36	1·64	0·01	0·06	0·13	4·20	4·56	49·92	0·11	0·02	0·00	0·00
FeO	85·90	21·22	17·30	86·67	83·50	80·29	86·42	85·56	22·67	12·55	14·09	7·54	8·10
MnO	0·06	0·19	0·10	0·30	0·52	0·40	0·00	0·00	0·53	0·43	0·46	0·29	0·35
NiO	0·36	0·11	0·38	0·00	0·00	0·09	0·11	0·00	0·10	0·28	0·25	0·59	0·39
MgO	0·20	14·67	15·53	0·54	0·67	1·56	0·19	0·26	7·82	45·15	44·01	50·05	50·00
V_2O_5	n.d.	n.d.	n.d.	n.d.	n.d.	n.d.	1·19	1·01	0·00	0·09	0·07	0·00	0·01
ZnO	0·00	0·10	2·51	n.d.	n.d.	n.d.	n.d.	n.d.	n.d.	n.d.	n.d.	n.d.	n.d.
Total	93·03	99·21	97·35	92·92	93·24	93·59	94·14	95·29	97·22	99·62	99·47	100·55	100·70
O = 4													
Si	0·008	0·009	0·001	0·008	0·007	0·000	0·006	0·005	0·000	1·028	1·026	1·019	1·014
Ti	0·012	0·004	0·001	0·108	0·166	0·132	0·028	0·083	0·007	0·000	0·000	0·002	0·000
Al	0·025	1·909	1·892	0·065	0·112	0·278	0·040	0·037	0·625	0·000	0·000	0·000	0·000
Cr	0·003	0·003	0·035	0·000	0·002	0·004	0·127	0·136	1·318	0·001	0·000	0·000	0·000
Fe^{3+}	1·112	0·062	0·069	1·055	1·004	0·974	1·047	1·016	0·041	0·000	0·000	0·000	0·000
Fe^{2+}	1·807	0·515	0·320	1·723	1·653	1·511	1·708	1·683	0·592	0·264	0·298	0·153	0·164
Mn	0·000	0·007	0·002	0·010	0·017	0·012	0·000	0·000	0·015	0·009	0·010	0·006	0·007
Ni	0·006	0·007	0·008	0·000	0·000	0·003	0·003	0·000	0·003	0·006	0·005	0·012	0·008
Mg	0·010	0·479	0·622	0·031	0·038	0·086	0·011	0·015	0·390	1·690	1·659	1·809	1·806
V	0·000	0·000	0·000	0·000	0·000	0·000	0·030	0·025	0·000	0·002	0·002	0·000	0·000
Zn	0·000	0·000	0·000	0·050									
Total	3·000	3·000	3·000	3·000	3·000	3·000	3·000	3·000	2·992	3·000	3·000	3·000	3·000

n.d., not determined.

Table 6: Selected electron microprobe analyses of amphibole

Rock type:	Garnet–clinopyroxene rocks				Garnetite		Harzburgite		
Mineral:	Pargasite						Tremolite		
Sample:	RH86-06	RH86-06	RH85-08	RH85-08	RH86-01	RH85-16	RH85-04	RH85-04	RH85-04
Position:	Matrix	Matrix	In Cpx	Lamellar	Matrix	Matrix	Matrix	Matrix	Matrix
SiO_2	42·19	42·83	43·71	44·96	41·10	43·19	46·79	58·15	56·69
TiO_2	0·12	0·20	0·27	0·10	0·39	0·17	0·14	0·04	0·02
Al_2O_3	16·29	15·11	14·27	12·71	15·72	13·54	11·71	0·78	2·10
Cr_2O_3	0·31	0·12	0·21	0·04	0·00	0·07	1·90	0·36	0·27
FeO	4·70	5·09	4·54	4·90	8·62	6·23	2·47	1·78	1·86
MnO	0·09	0·11	0·07	0·03	0·10	0·00	0·12	0·15	0·12
NiO	1·33	0·00	0·03	0·14	0·09	0·05	0·09	0·13	0·01
MgO	17·29	18·67	18·38	16·31	15·28	17·63	20·28	23·49	23·14
CaO	12·21	11·91	12·93	15·18	12·87	12·06	11·32	12·95	12·69
Na_2O	3·59	3·20	2·95	2·17	2·93	2·03	2·40	0·23	0·58
K_2O	0·21	0·27	0·77	0·26	0·23	1·56	0·39	0·00	0·01
F	n.d.	n.d.	n.d.	n.d.	n.d.	n.d.	0·03	0·00	0·00
Cl	n.d.	n.d.	n.d.	n.d.	n.d.	n.d.	0·07	0·06	0·04
Total	98·33	97·51	98·11	96·80	97·35	96·53	97·71	98·12	97·53
O = 23									
Si	5·980	6·098	6·204	6·576	5·986	6·299	6·572	7·930	7·791
Ti	0·013	0·021	0·029	0·010	0·043	0·019	0·015	0·004	0·002
Al^{IV}	2·020	1·902	1·796	1·424	2·014	1·701	1·428	0·070	0·209
Al^{VI}	0·701	0·634	0·593	0·767	0·685	0·627	0·511	0·056	0·131
Cr	0·035	0·014	0·024	0·005	0·000	0·008	0·211	0·039	0·029
Fe^{3+}	0·282	0·144	0·072	0·000	0·116	0·000	0·000	0·000	0·000
Fe^{2+}	0·275	0·462	0·467	0·599	0·935	0·760	0·290	0·203	0·214
Mn	0·011	0·013	0·008	0·003	0·013	0·000	0·014	0·017	0·014
Ni	0·152	0·000	0·003	0·017	0·011	0·006	0·010	0·014	0·001
Mg	3·652	3·962	3·888	3·556	3·317	3·832	4·245	4·774	4·739
Ca^{M4}	1·854	1·817	1·966	2·378	2·009	1·885	1·704	1·892	1·869
Na^{M4}	0·038	0·000	0·000	0·000	0·000	0·000	0·015	0·004	0·002
Na^{A}	0·949	0·884	0·811	0·615	0·829	0·574	0·639	0·057	0·153
K^{A}	0·038	0·049	0·139	0·049	0·043	0·290	0·070	0·000	0·002
V^{A}	0·013	0·067	0·049	0·335	0·128	0·135	0·291	0·943	0·846
Σcations	16·000	16·000	16·000	16·000	16·000	16·000	15·724	15·061	15·156

correlated and Cr and Ni positively correlated with Mg/(Mg + Fe) (Fig. 6). Type I Grt–Cpx rocks (e.g. RH86-10) are relatively low in Mg and Cr, and high in Ti, Fe, and light rare earth elements (LREE) (Tables 1 and 2). Some type II Grt–Cpx rocks have compositions similar to those of type I (Table 1). Diopsidite has the highest Mg, Cr and Ni, and lowest Ti and Fe contents.

The REE abundances in the Grt–Cpx rocks are in the range of 1–30 times C1 chondrite. They are positively correlated with Fe and Ti. Their chondrite-normalized REE patterns are convex upward (Fig. 7a) and mimic that of clinopyroxene (Jahn, 1999), suggesting that their protoliths were clinopyroxenites. Compared with normal mid-ocean ridge basalts (MORB) (Hofmann, 1988), the rocks are significantly enriched in Ba, Ti, Co, Mg, Ni, and Cr, slightly depleted in LREE, increasingly depleted from middle REE (MREE) to heavy REE (HREE), and strongly depleted in K, P, Nb, and Zr (Fig. 7b). Serpentinite and harzburgite are very low in Al, Ti, Ca, and Na. A sample of serpentinite (RH85-701)

Table 7: LAM-ICP-MS analyses of trace elements in clinopyroxene and garnet

Sample:	RH86-12	RH86-16	RH86-16
Mineral:	Cpx	Cpx	Garnet
La	2·46	1·29	0·01
Ce	13·52	5·88	0·14
Pr	2·60	1·18	0·09
Nd	13·7	6·5	1·4
Sm	2·61	1·18	1·78
Eu	0·72	0·27	0·90
Gd	1·11	0·55	2·74
Tb	0·08	0·02	0·57
Dy	0·25	0·13	3·75
Ho	0·03	0·02	0·92
Er	0·04	0·03	2·80
Tm	<0·01	0·005	0·379
Yb	0·07	0·03	2·50
Lu	0·010	0·011	0·313
Rb	0·16	0·07	<0·09
Ba	0·4	2·6	0·0
Ga	8·32	7·17	7·62
Th	0·010	0·021	0·003
U	0·013	0·005	0·003
Ta	<0·016	<0·01	<0·023
Nb	0·01	0·02	0·01
Sr	120·3	111·5	0·2
Zr	12·6	5·0	12·2
Y	0·45	0·30	23·57
Sc	39	29	139
V	157	160	147
Hf	1·03	0·47	0·34
Co	29	24	48
Ni	35	163	8
Cr	33	415	1185

enclosing the Grt–Cpx rocks displays a large negative Eu anomaly, whereas the other sample (RH85-702b) collected from the middle of the large serpentinite body east of Hujialin (Fig. 1) lacks a Eu anomaly. All the ultramafic rocks have $La_N/Yb_N > 1$.

MINERAL MAJOR ELEMENT COMPOSITIONS

Garnet

Variation of garnet composition is mainly in the relative proportions of the pyrope and grossular components (Table 3, Fig. 8). Although the entire compositional range is continuous, garnet in many samples falls into two distinctly different populations. One population is represented by $Prp_{33–42}Alm_{21–26}Gro_{37–40}Spe_{0–1}$, which includes the compositions of the cores of garnet porphyroblasts in some samples, megacrystic garnet containing clinopyroxene or ilmenite inclusions, and the garnet lamellae rarely found in the clinopyroxene inclusions. Another population is represented by $Prp_{18–23}Alm_{20–23}Gro_{56–60}Spe_{0–1}$, including the compositions of garnet lamellae exsolved from clinopyroxene, core to rim of garnet porphyroblasts in some samples, aggregates of fine-grained garnet in the matrix, and some coarse-grained garnet bearing rutile needles. The grossular content of the garnet displays a generally positive correlation with the Alm/Prp ratio. Garnet in some samples contains appreciable amounts of Na. For example, the Na_2O content in the coarse-grained Ca-rich garnet in sample RH86-01 is 0·03–0·12 wt %, with an average of 0·075 ± 0·024 (1σ) wt %.

Garnet porphyroblasts are in places rimmed by a new generation of fine-grained garnet, which is brighter in the BSE images (Fig. 4f), displaying sharp contact boundaries. Such garnet rims are enriched in Ca and Mn to different extents relative to their cores. In places, the contacts are diffuse, where Ca and also Mn contents increase and Mg content decreases substantially towards the rim. Hiramatsu & Hirajima (1995) reported the most Ca- and Mn-rich and Mg-poor composition ($Prp_5Alm_{22}Gro_{70}Spe_3$) at the outermost rim of a garnet grain (Fig. 8).

Pyroxene

Coarse-grained clinopyroxene in the Grt–Cpx rocks is higher in Al, Na, Cr, and Ti (Fig. 9), and lower in Mg [$X_{Mg} = Mg/(Mg + Fe) = 0·88–0·92$] (taking all Fe as Fe^{2+}), Ca, and Si, compared with the fine-grained diopside ($X_{Mg} = 0·92–0·94$) (Table 4). The highest Al_2O_3 content in a large clinopyroxene grain with less extensive garnet exsolution lamellae is 5·06 wt %, with a minimum X_{Mg} of 0·90. Many clinopyroxene analyses have $Al^{IV}/Al^{VI} > 1$, reflecting their original igneous compositional characteristics (e.g. Debari & Coleman, 1989). A compositional trend from close to the precursor augite with high Ti contents toward high Na and Al compositions is formed by the residual clinopyroxene after different extents of exsolution (Fig. 9), with the fine-grained diopside highest in Na and Al, indicating a higher jadeite component (up to 5 mol %). In terms of Ca–Mg–Fe, the clinopyroxene compositions reported earlier (Hiramatsu & Hirajima, 1995; Zhang *et al.*, 2000) and in this study mostly plot in the field for diopside (Fig. 10), with a few analyses falling well above the 50% Ca line of the pyroxene quadrilateral.

Orthopyroxene in harzburgite is Al- and Cr-poor and subtly zoned in composition, with Al increasing and X_{Mg} decreasing from the cores (≥0·17 wt % Al_2O_3 and *c.* 0·93, respectively) to the rims (≤0·97 wt % Al_2O_3 and *c.* 0·92, respectively).

Olivine, spinel, and ilmenite

Olivine inclusions ($Fo_{86–87}$) in diopside are more enriched in Mg relative to olivine in the matrix ($Fo_{84–85}$), both having low NiO contents (≤0·3 wt %). Hiramatsu & Hirajima (1995) reported a slightly more Mg-rich olivine inclusion (Fo_{89}) in garnet and a less Mg-rich matrix olivine (Fo_{80}), whereas Zhang *et al.* (2000) reported compositions of olivine both in the matrix and garnet ranging from Fo_{83} in the cores to Fo_{70} in the rims. Olivine composition in the harzburgite is around Fo_{92}, with NiO contents ranging from 0·2 to 0·6 wt %.

The compositions of the green spinel that occur inside or at the boundary of garnet fall on the spinel–hercynite join, and vary from close to $Spl_{50}Hrc_{50}$ (Table 5) to $Spl_{61–73}Hrc_{39–27}$ (Hiramatsu & Hirajima, 1995; Zhang *et al.*, 2000). In most samples, magnetite is enriched in Ti (Table 5), more so in the cores of large grains. Appreciable amounts of V and Zn are detected in otherwise pure magnetite in some samples, whereas magnetite in other samples is enriched in Cr. Chromite in the harzburgite is mainly a solid solution between chromite and spinel, with <10 mol % of picrochromite. Ilmenite grains in the Grt–Cpx rock matrix are richer in Mg ($Gkl_{12}Ilm_{88}$; where Gkl is geikielite, and Ilm is ilmenite) than those included in garnet (Gkl_5Ilm_{95}), which are slightly more enriched in Mg than the ilmenite lamellae in augite (Gkl_3Ilm_{97}) (Table 3).

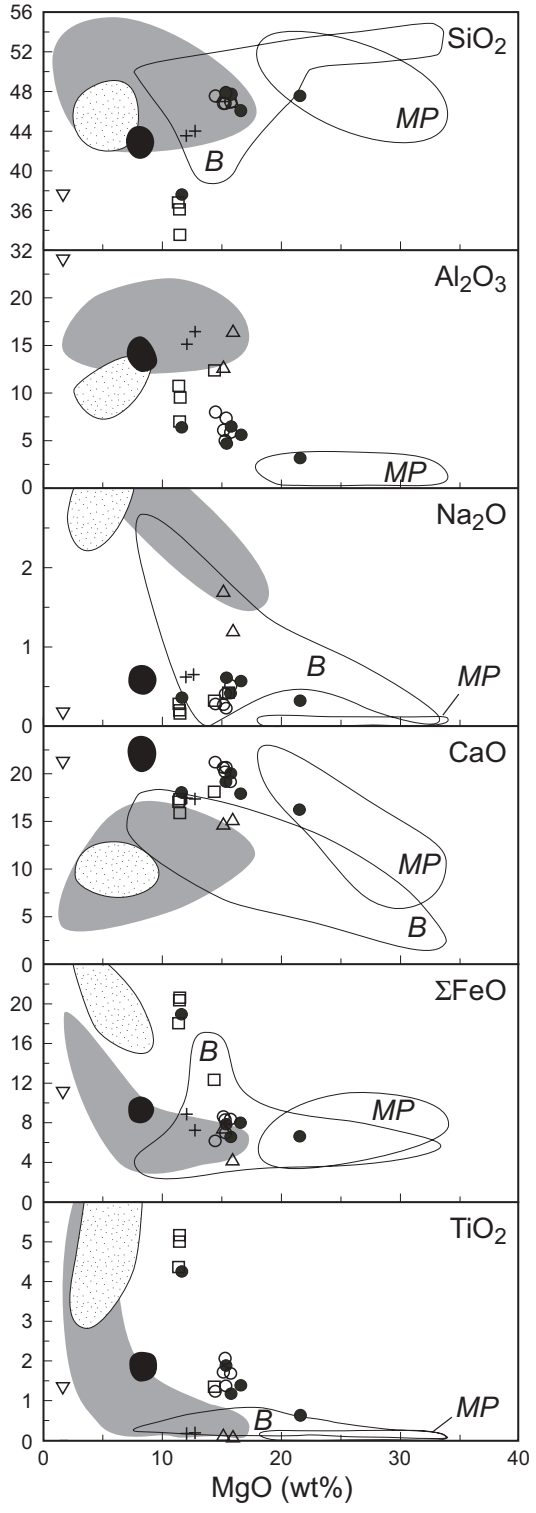

Fig. 5. Major element oxides vs MgO (wt %) for the Hujialin Grt–Cpx whole-rocks. ●, this study; □, Yang (1991); ○, Jahn (1999). Similar assemblages from other localities are also shown. △, Scharbert & Carswell (1983); ▽, Vrána & Frýda (2003); +, xenoliths in kimberlite (Harte & Gurney, 1975); *B*, field for data from Becker (1996); *MP*, field for data on pyroxenites in supra-subduction zone ophiolites (Melcher *et al.*, 2002; Parlak *et al.*, 2002). Grey field indicates oceanic gabbros (Holm, 2002); dotted field, Fe–Ti gabbros (Scambelluri & Rampone, 1999, and references therein); black field, Grt–Cpx rocks from Rushan, north Su–Lu terrane (Yang *et al.*, 2005).

Amphibole, titanite, epidote, chlorite and talc

Amphibole in the Grt–Cpx rocks is pargasitic; it is higher in Na^{M4} in the rock matrix than amphibole inclusions in clinopyroxene (Table 6). Amphibole in Ca-rich garnetite is higher in Fe than in the other Grt–Cpx rocks. Amphibole in the harzburgite is mainly actinolite, that replacing orthopyroxene is higher in Al, and some analyses are pargasite.

Coarse-grained titanite coexisting with epidote and amphibole is very close to pure $CaTiSiO_5$, with negligible $(Al,Fe^{3+})(F,OH)Ti_{-1}O_{-1}$ substitution. Both epidote and zoisite occur in the Grt–Cpx rocks as retrograde minerals replacing garnet. The rim of zoisite is slightly higher in Fe. Chlorite in Grt–Cpx rocks varies in X_{Mg} in different samples, with that in the Ca-rich garnetite being the lowest. Chlorite in harzburgite is the highest in X_{Mg} and contains significant amounts of Cr. Talc in the harzburgite is low in Fe and Al.

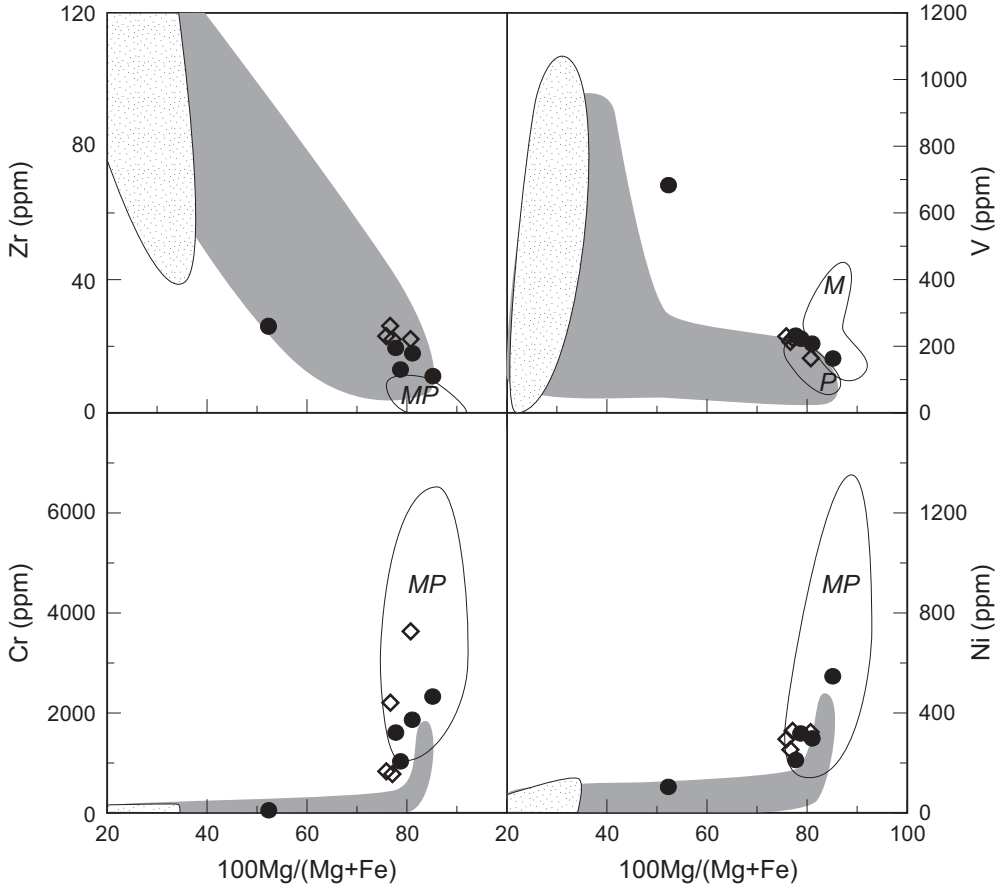

Fig. 6. Whole-rock trace elements vs 100Mg/(Mg + Fe). ●, This study; ◇, Jahn (1999). The fields are as in Fig. 5.

MINERAL TRACE ELEMENT COMPOSITIONS

Clinopyroxene shows convex upward chondrite-normalized REE patterns, with Pr and Nd 10–30 times and HREE 0·2–0·4 times chondrite (Fig. 7a). Clinopyroxene inclusions in garnet have systematically lower trace element contents than the exsolution lamellae-bearing large clinopyroxene grains, except for Ba, Ni, and Cr, which are significantly higher in the clinopyroxene inclusions (Table 7). Garnet is depleted in LREE but is enriched in MREE to HREE and has a flat chondrite-normalized REE pattern.

DISCUSSION

Origin of the Grt–Cpx rocks: geochemical and isotope evidence

The Hujialin Grt–Cpx rocks are at the low-MgO and high-CaO end of the compositional spectrum of pyroxenites from supra-subduction zone ophiolites (Melcher *et al.*, 2002; Parlak *et al.*, 2002) and from garnet peridotite massifs in Austria (Becker, 1996) (Fig. 5). With the exception of TiO_2, they exhibit a range of variation in whole-rock composition similar to that of the Austrian garnet pyroxenites. Their Ca-rich and Na-poor whole-rock compositions are consistent with an origin as cumulate clinopyroxenites. Most of the samples lie on a compositional trend from high-Mg cumulates to gabbros (Fig. 5). This, together with the high total Fe and Ti contents, indicates that they were cumulates not from primary magmas in equilibrium with mantle peridotite, but from evolved magmas after variable amounts of differentiation in which magnetite crystallization was suppressed (e.g. Miyashiro & Shido, 1975). Fractional crystallization of olivine and low-Al clinopyroxene from primary magmas produces lower Mg/(Mg + Fe) and higher Al magmas (e.g. DeBari & Coleman, 1989). Diopsidites near the boundary with the enclosing serpentinite were probably derived from cumulates of less evolved magmas, whereas type I and some type II garnet-rich rocks near the centre of the Grt–Cpx rock body seem to have been derived from cumulates of more evolved magmas.

The Grt–Cpx rocks are generally depleted in incompatible elements such as Rb, Sr, and LREE relative to

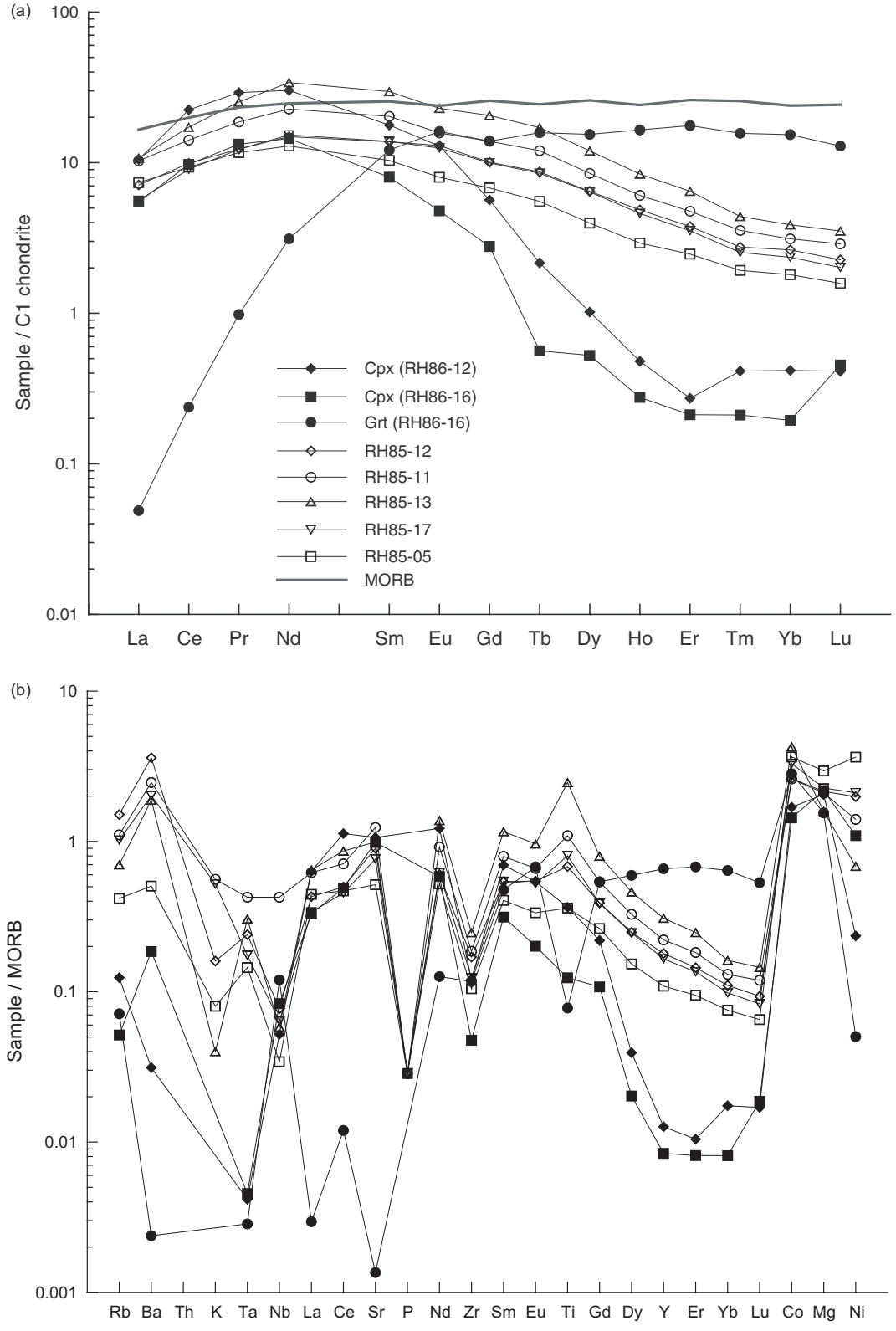

Fig. 7. Normalized trace element characteristics of Grt–Cpx rocks, clinopyroxene, and garnet. (a) Chondrite-normalized REE patterns. Data for C1 chondrite are from Anders & Grevesse (1989). Data for N-MORB from Hofmann (1988). (b) MORB-normalized multi-element patterns. Legends are as in (a).

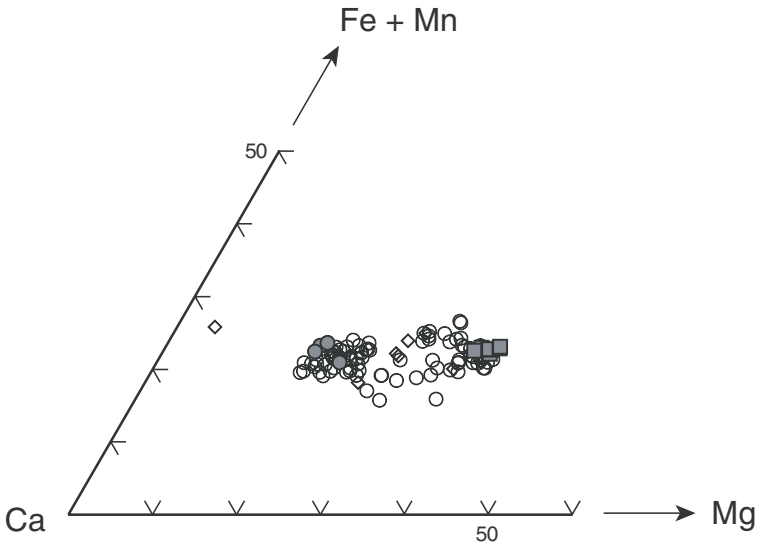

Fig. 8. (Fe + Mn)–Ca–Mg cation proportions of garnet. ○, Garnet compositions from this study; filled squares (Grt1), cores of large garnet and megacrystic garnet (RH86-16); ● (Grt2), lamellae in augite and small grains in matrix (RH85-08); diamond, garnet compositions from Hiramatsu & Hirajima (1995).

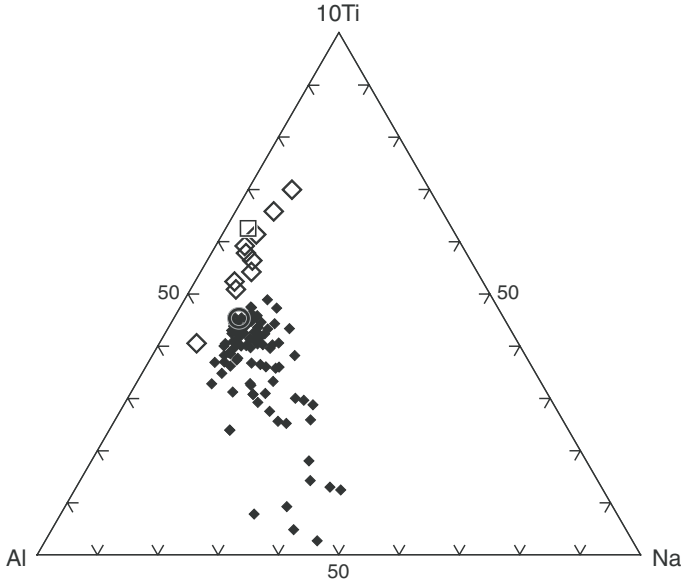

Fig. 9. Ti–Al–Na cation proportions of clinopyroxene. ♦, Clinopyroxene analyses from this study. Large open symbols are reconstructed precursor augite; ◇, this study; ○, Hiramatsu & Hirajima (1995); □, Zhang & Liou (2003).

MORB, but are enriched in compatible elements such as Cr, Co, and Ni. Such compositions cannot be produced directly by the partial melting of mantle peridotite, but can be formed by crystal accumulation from mantle-derived melts (Suen & Frey, 1987). Correlations between trace elements and Mg/(Mg + Fe) (Fig. 6) are similar to the trends of arc cumulates crystallized from fractionated tholeiitic magmas (Debari & Coleman, 1991; Müntener *et al.*, 2001).

The type I and some of the type II Grt–Cpx rock samples plot away from the main trends in the SiO_2 and TiO_2 vs MgO diagrams (Fig. 5). Their very low Mg/(Mg + Fe) ratios and high total Fe and Ti contents suggest the presence of cumulus magnetite and ilmenite in the protolith. Local concentrations of these minerals may result in the compositional variation away from the igneous trend. The low Si and high Al contents of these Grt–Cpx rocks are also related to their higher modal contents of garnet and spinel. The Al-rich spinel occurring as granular inclusions in garnet was likely to have been present in the igneous protoliths. The lack of a Eu anomaly and absence of textural evidence for the

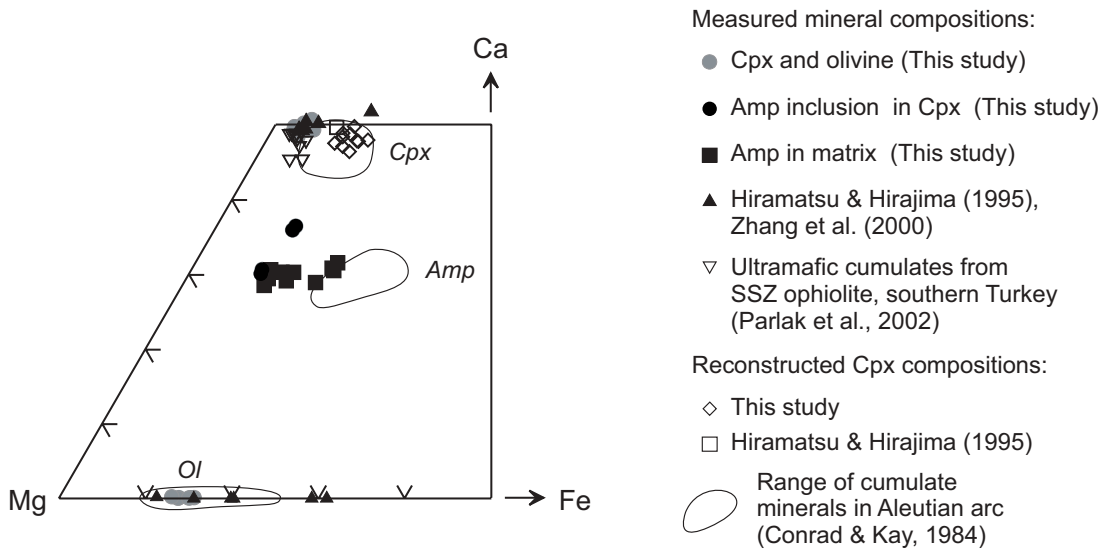

Fig. 10. Ca–Mg–Fe cation proportions of clinopyroxene, amphibole and olivine in Hujialin Grt–Cpx rocks and cumulates from other localities.

former presence of plagioclase indicates that the protoliths were not gabbroic. The significant depletion in the immobile incompatible elements Zr, Y and HREE in the Grt–Cpx rocks relative to MORB may also be related to the cumulate nature of a protolith mainly composed of augite and spinel with negligible (if any) igneous garnet.

Zhang *et al.* (2000) reported oxygen isotope data ($\delta^{18}O$ = 4·83–5·64‰ for garnet, $\delta^{18}O$ = 4·99–5·64‰ for clinopyroxene) for the Hujialin Grt–Cpx rocks. Some values are appreciably lower than that of the mantle ($\delta^{18}O$ = 5–7‰), indicating either a high-level crustal history, e.g. rodingitization (Rösli *et al.*, 1991), or a relation to subduction zone metasomatism. Jahn (1999) estimated their initial $^{87}Sr/^{86}Sr$ ratios and $\varepsilon_{Nd}(220)$ values to be in the range 0·7032–0·7036 and +1·2 to +2·9, respectively, consistent with a cumulate origin in the mantle. The $\varepsilon_{Nd}(220)$ values are lower than expected for mantle-derived rocks, which may suggest input of a continental crustal component into their mantle source, possibly from subducted sediments.

The Grt–Cpx rock enclosed in eclogite from north Su–Lu described by Yang *et al.* (2005) is even higher in CaO than the Hujialin rocks. Its protolith is roughly a monomineralic clinopyroxenite enclosed within a gabbro (now eclogite). An extremely low Mg/(Mg + Fe) ratio suggests that it also represents a cumulate from a differentiated magma. It is possible that similar mineral assemblages in other orogenic belts may have similar origins. The Ca-rich Grt + Cpx assemblages from kimberlites (O'Hara & Mercy, 1966; Harte & Gurney, 1975) also share such mineralogical and petrological characteristics, and may also represent recycled cumulates.

Origin of Grt–Cpx rocks: mineral chemistry evidence

Garnet locally forms aggregates, recrystallized into garnetites with both Mg-rich (RH86-16) and Ca-rich (RH86-01 and RH85-16) compositions, with relict clinopyroxene (rarely containing garnet lamellae) in the more Mg-rich garnet megacrysts, and fine-grained diopside between Ca-rich garnet aggregates. The spinel and clinopyroxene inclusions in garnet porphyroblasts indicate that the garnet cores formed at the expense of these minerals after the igneous stage.

Exsolution of garnet, ilmenite, magnetite, and spinel would have removed Al, Ti, and Fe from the precursor augite, whereas almost all the Na, and much of the Ca, Mg, and Si remained in the host grain to form diopside (Fig. 9). Reconstruction of precursor clinopyroxene compositions for the Hujialin clinopyroxenites was attempted for samples RH86-08 and RH86-12, based on BSE imaging (0·38 mm × 0·53 mm) of the interiors of 10 garnet- and oxide-bearing clinopyroxene grains. As the proportions of exsolution lamellae are variable, with garnet ranging from 2·3 to 21·7 vol. %, spinel from 0 to 1·7 vol. %, and opaque minerals from 1·8 to 4·6 vol. %, the reconstructed clinopyroxene compositions are variable (Table 8). In addition, because of the difficulty in distinguishing ilmenite from magnetite, estimates of their proportions in the exsolution texture are imprecise.

Assuming that the molar proportions of ilmenite and magnetite are 1:1, the reconstructed Ca–Mg–Fe compositions of the precursor clinopyroxene fall into the field of clinopyroxene in ultramafic cumulates beneath island arcs (Conrad & Kay, 1984; Debari & Coleman, 1989; Parlak *et al.*, 2002) (Fig. 10). They are

Table 8: Reconstruction of precursor clinopyroxene compositions from exsolution lamellae

	Compositions of minerals in exsolution texture					Reconstructed clinopyroxene compositions with Mag:Ilm ~1:1										HH95*	ZL03*
Sample:	RH86-12				RH86-03	RH86-08a	RH86-08b	RH86-08c	RH86-08d	RH86-12a	RH86-12b	RH86-12c	RH86-12d	RH86-12e	RH86-12f		
Mineral:	Cpx	Grt	Hrc	Mag	Ilm												
No. av.:	6	4	1	2	1												
SiO_2	53·24	39·97	0·41	0·05	0·10	49·02	50·51	50·39	48·89	49·06	50·33	49·61	48·16	50·24	49·31	50·83	48·66
TiO_2	0·34	0·38	0·05	3·37	51·33	1·55	1·56	1·03	1·42	0·85	1·14	1·13	1·62	0·99	1·62	0·87	1·69
Al_2O_3	2·90	21·10	57·82	0·91	0·00	5·33	3·25	4·54	5·75	7·19	4·67	5·68	6·31	5·20	4·41	5·42	5·83
Cr_2O_3	0·05	0·04	3·02	0·04	0·00	0·05	0·05	0·11	0·07	0·06	0·05	0·05	0·05	0·05	0·10	0·00	0·02
Fe_2O_3	2·09	1·52	3·05	37·49	0·00	2·76	2·83	2·52	2·68	2·27	2·53	2·49	2·77	2·42	2·88	0·00	5·99
FeO	0·81	8·13	22·06	55·33	45·84	4·06	3·24	2·76	3·99	3·49	3·02	3·41	4·58	2·96	3·83	4·38	
MnO	0·05	0·59	0·52	0·24	1·37	0·16	0·10	0·10	0·16	0·19	0·13	0·16	0·19	0·14	0·12	0·10	0·19
NiO	0·00	0·00	0·57	0·00	0·06	0·00	0·00	0·01	0·00	0·00	0·00	0·00	0·00	0·00	0·01	0·00	0·00
MgO	16·30	6·41	12·10	0·42	0·81	14·22	15·34	15·44	14·22	13·70	14·83	14·29	13·64	14·63	15·09	14·44	13·98
CaO	24·15	21·85	0·00	0·00	0·00	22·75	23·00	22·99	22·71	23·12	23·20	23·08	22·56	23·27	22·51	23·12	23·80
Na_2O	0·68	0·00	0·00	0·00	0·00	0·55	0·63	0·62	0·55	0·51	0·59	0·55	0·51	0·57	0·61	0·82	0·39
Total	100·40	99·83	99·59	97·84	99·50	100·25	100·31	100·32	100·25	100·24	100·29	100·26	100·21	100·29	100·28	99·98	100·55
Si	1·923	3·001	0·011	0·002	0·003	1·803	1·851	1·837	1·797	1·798	1·841	1·818	1·777	1·837	1·809	1·857	1·784
Ti	0·009	0·022	0·001	0·096	0·972	0·043	0·043	0·028	0·039	0·024	0·031	0·031	0·045	0·027	0·045	0·024	0·047
Al	0·123	1·867	1·848	0·041	0·000	0·231	0·140	0·195	0·249	0·310	0·202	0·246	0·274	0·224	0·191	0·233	0·252
Cr	0·002	0·002	0·065	0·001	0·000	0·001	0·001	0·003	0·002	0·002	0·001	0·001	0·001	0·001	0·003	0·000	0·001
Fe^{3+}	0·057	0·086	0·062	1·071	0·050	0·113	0·115	0·114	0·115	0·080	0·094	0·092	0·116	0·086	0·140	0·063	0·112
Fe^{2+}	0·025	0·513	0·500	1·758	0·915	0·089	0·063	0·040	0·083	0·090	0·069	0·081	0·104	0·071	0·058	0·071	0·073
Mn	0·002	0·038	0·012	0·008	0·029	0·005	0·003	0·003	0·005	0·006	0·004	0·005	0·006	0·004	0·004	0·003	0·006
Ni	0·000	0·000	0·012	0·000	0·001	0·000	0·000	0·000	0·000	0·000	0·000	0·000	0·000	0·000	0·000	0·000	0·000
Mg	0·877	0·717	0·489	0·023	0·030	0·780	0·838	0·839	0·779	0·748	0·808	0·780	0·750	0·797	0·825	0·786	0·764
Ca	0·935	1·757	0·000	0·000	0·000	0·897	0·903	0·898	0·894	0·908	0·909	0·907	0·892	0·912	0·885	0·905	0·935
Na	0·047	0·000	0·000	0·000	0·000	0·039	0·045	0·044	0·039	0·036	0·042	0·039	0·037	0·041	0·043	0·058	0·028
Total	4·000	8·002	3·000	3·000	2·000	4·002	4·002	4·001	4·002	4·001	4·001	4·001	4·002	4·001	4·002	4·001	4·002

*HH95 and ZL03 are reconstructed clinopyroxene precursor compositions by Hiramatsu & Hirajima (1995) and Zhang & Liou (2003), respectively.

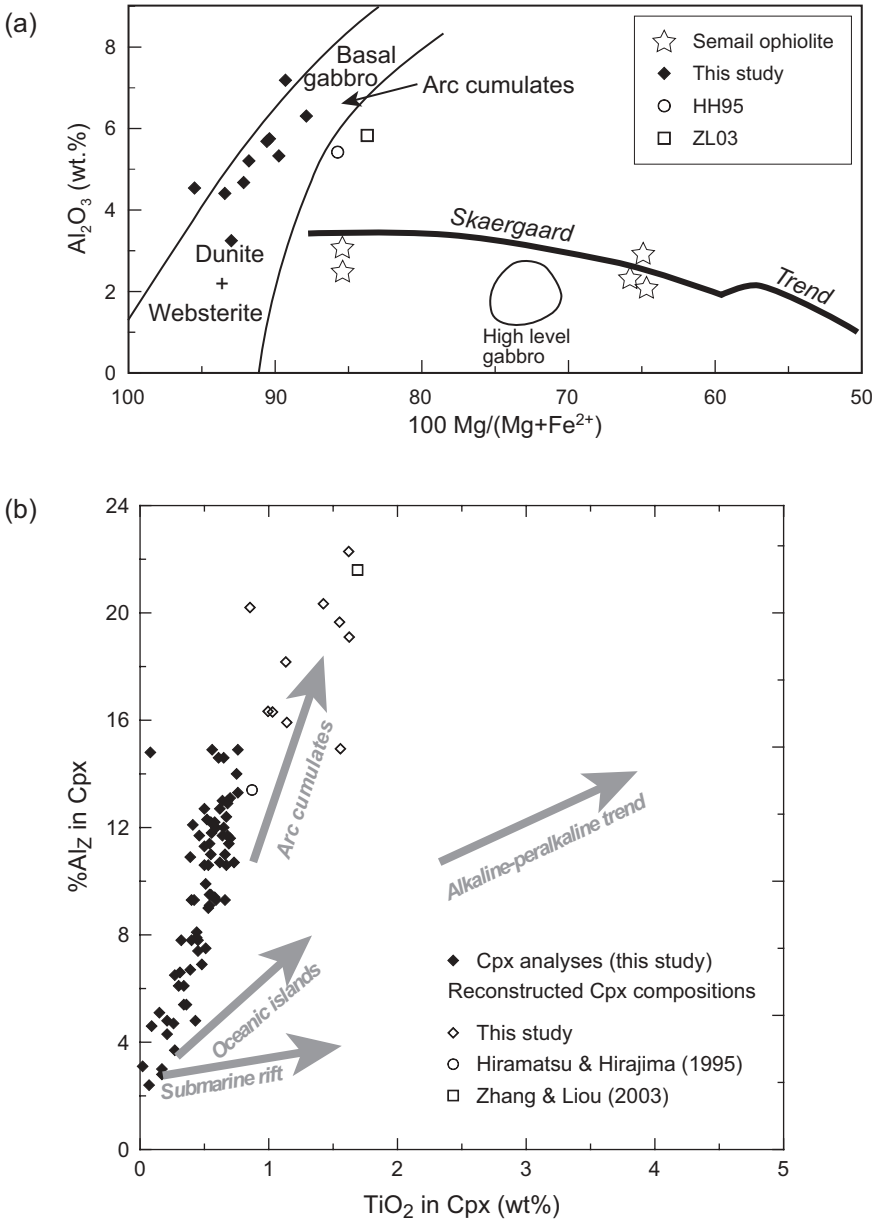

Fig. 11. Comparison of reconstructed clinopyroxene compositions with those of arc cumulates. (a) Al_2O_3 vs $100Mg/(Mg + Fe^{2+})$. Compositional ranges for arc cumulates, Semail ophiolite, high-level gabbro, and Skaergaard trend are all from DeBari & Coleman (1989). HH95, Hiramatsu & Hirajima (1995); ZL03, Zhang & Liou (2003). (b) $\%Al_Z$ vs wt % TiO_2 in Cpx; $\%Al_Z$ is the percentage of Al on the tetrahedral site of clinopyroxene. Compositional trends are from Loucks (1990).

also roughly within the array for clinopyroxene in arc cumulates in an Al_2O_3 vs $Mg/(Mg + Fe^{2+})$ diagram (Fig. 11a), consistent with magma differentiation as a result of fractional crystallization of olivine and low-Al and high-X_{Mg} clinopyroxene.

Igneous clinopyroxene with high Al^{IV}/Ti ratios is characteristic of subduction-related cumulates (Loucks, 1990). The clinopyroxene analyses in the Hujialin Grt–Cpx rocks form an array slightly steeper than the trend for arc cumulates, with lower Ti contents (Fig. 11b). Given that the clinopyroxene compositions are metamorphic and mostly represent residues from exsolution of minerals including Fe–Ti oxides, their igneous precursors must have been richer in Ti. The reconstructed augite compositions in this study and those by Hiramatsu & Hirajima (1995) and Zhang & Liou (2003) plot well within the array for arc cumulates, although the tetrahedral Al contents in some samples are higher than those recorded by Loucks (1990) as a result of magmatic differentiation.

Considerable amounts of Fe^{3+} (or esseneite component) are implied by the presence of magnetite exsolution lamellae in the igneous augite; amphibole lamellae in some clinopyroxene grains may suggest hydroxyl in the precursor augite. These are typical features of clinopyroxene in island-arc cumulates (Loucks, 1990). Chen *et al.* (2003) also reported pargasite and ilmenite lamellae in clinopyroxene from Hujialin. They showed coherent lattice interfaces between the pargasite and the host clinopyroxene, and concluded that the pargasite was formed by exsolution from the clinopyroxene. Using the volume data of Holland & Powell (1998), the *c.* 14 vol. % of pargasite in Fig. 4d translates into *c.* 3·8 mol %; hence, the amount of H_2O in this grain is about 2900 ppm. Given the low partition coefficient (0·01–0·03) for H_2O between clinopyroxene and basaltic magma (Hauri *et al.*, 2004), it is questionable if all these amphibole lamellae are the products of exsolution from the host augite. On the other hand, the fact that pargasite occurs only inside and not on the boundaries of the host clinopyroxene (Fig. 4c and d) indicates that it crystallized during cooling from the igneous stage, precluding the possibility that it resulted from ingress of external fluid during late-stage exhumation. Therefore, the pargasite lamellae in clinopyroxene are either the products of exsolution or prograde inclusions. The local preservation of such amphibole lamellae in clinopyroxene, along with spinel in garnet, at Hujialin indicates that they survived UHP metamorphism. A similar case involving preservation of prograde amphibole in clinopyroxene was described for a UHP garnet lherzolite at Zhimafang in the southern Su–Lu terrane (Yang, 2003).

According to Gust & Perfit (1987), Cpx ± Ol are liquidus phases in anhydrous high-Mg island arc basalts at 0·5–1 GPa. Amphibole becomes a near-liquidus phase when the water content of the system is high (Conrad & Kay, 1984; Müntener *et al.*, 2001). The pargasite inclusions in clinopyroxene, therefore, imply elevated P_{H_2O} during the igneous stage of the Hujialin Grt–Cpx rocks.

The composition of olivine ($Fo_{89–70}$) and its modal abundance (≤15 vol. %) are typical of cumulates produced by crystal fractionation from mafic melts (Conrad & Kay, 1984). The green spinel containing considerable amount of hercynite is often found in mafic–ultramafic cumulates (Conrad & Kay, 1984; Melcher *et al.*, 2002).

Mineral assemblages of Ca-rich Grt + Di + Ilm + Mag ± Ol ± Ep ± Ttn ± Amp, similar to those at Hujialin, have previously been described as metarodingites in the Central Alps, where former oceanic basalts and gabbros were subjected to rodingitization before being metamorphosed at high pressure (Evans *et al.*, 1979). The very high CaO contents (>15 wt %) and very low Na_2O and SiO_2 contents (<1 wt % and <48 wt %, respectively) of the Hujialin Grt–Cpx rocks are well within the range of rodingites. However, no relict mineral characteristic of rodingite (such as prehnite, vesuvianite, etc.) (e.g. Rösli *et al.*, 1991) has been observed, thus providing no mineralogical evidence for rodingitization before UHP metamorphism. The minor Ca enrichment at garnet rims cannot account for the overall Ca-rich compositions of the rocks. On the other hand, the reconstructed precursor clinopyroxene compositions plot well within the compositional field of cumulates. Therefore, the Ca-rich composition of the protoliths of the clinopyroxenites can explain the Ca-rich nature of the UHP Grt–Cpx rocks.

Compositional characteristics of the ultramafic rocks

The serpentinite and harzburgite are high in Mg and Cr, and low in Ti, Na, Ca and Al. These are characteristic features of refractory peridotites formed after the removal of large amounts of basaltic components. The low REE abundances of the harzburgite suggest earlier depletion in REE as a result of partial melting. Enrichment of LREE in the ultramafic rocks may be related to later interaction with fluids derived from the surrounding country rocks.

Although Mg–Fe partitioning between the constituent minerals may have been modified by high-pressure metamorphism, the high Mg and Ni contents in olivine and high Cr and Fe contents in chromite in the harzburgite must have been inherited from a depleted mantle protolith, consistent with an origin in a sub-arc mantle wedge (Dick & Bullen, 1984). Orthopyroxene in the harzburgite contains very little Al (<0·04 a.p.f.u.) and is enriched in Mg (X_{Mg} = 0·920–0·932), also suggesting a sub-arc depleted mantle origin (Koepke *et al.*, 2002).

Metamorphic evolution and *P–T* path

The presence of Al-spinel and absence of garnet and plagioclase in the igneous protoliths of the Hujialin Grt–Cpx rocks implies that the spinel clinopyroxenites crystallized at a depth near the crust–mantle transition zone. The 'Ca-in-olivine' geobarometer of Köhler & Brey (1990) was applied to an olivine inclusion in clinopyroxene in a sample of Grt–Cpx rock (RH86-06), assuming that it still retains its original Ca content in the cumulate protolith. This assumption is reasonable given that pargasite in clinopyroxene and spinel in garnet and clinopyroxene appear to have preserved their original composition through the UHP metamorphism. The barometer defines a *P–T* line at high temperatures (950–1100°C; Table 9), consistent with the suggestion that the olivine inclusion crystallized early in the igneous stage.

Whereas the presence of Al-rich spinel and clinopyroxene inclusions in garnet (Fig. 4e) is consistent with the

Table 9: P–T estimates of Hujialin garnet–clinopyroxene rocks

	Garnet–clinopyroxene geothermometry (Krogh Ravna, 2000)								
	RH86-16 Cpx inclusion/host Grt		RH86-06 Matrix Di/Grt core		RH85-08 Matrix Di/Grt core		RH86-12 Cpx/Center of Grt lamella		RH85-05
	I	II	I	II	I	II	I	II	
Pressure (GPa)									
1	650	550	675	600	610	450	770	550	
2	700	600	730	650	650	490	820	590	
3	750	650	780	700	690	520	870	630	
4	810	690	830	750	735	560	920	665	
5	860	740	885	790	780	595	970	705	
6	910	790	940	840	820	630	1020	740	
	Geobarometry								
	Spl–Grt	Al-in-Cpx	Spl–Grt	Al-in-Cpx	Spl–Grt	Al-in-Cpx	Spl–Grt	Al-in-Cpx	Ca-in-Ol
Temperature (°C)									
600	18·1	2·9	17·6	3·9	20·6	3·3	20·3	4·2	
700	19·4	3·4	18·9	4·7	22·2	4·0	21·9	4·9	
800	20·8	4·0	20·3	5·4	23·9	4·6	23·5	5·7	
900	22·3	4·6	21·7	6·1	25·7	5·3	25·2	6·5	
950	23·1	4·9	22·5		26·6	5·6	26·1		0·6
1000	23·9	5·2	23·2		27·5	6·0	27·0		1·1
1050		5·5				6·3			1·7
1100		5·8				6·6			2·6

I, ΣFe as Fe^{2+}; II, Fe^{3+}/Fe^{2+} corrected.

reaction

$$Ca_2(Fe,Mg)Al_2Si_3O_{12} + (Mg,Fe)_2SiO_4 = 2\ Ca(Mg,Fe)Si_2O_6 + (Fe,Mg)Al_2O_4 \quad (1)$$

the reaction

$$Ca_2MgAl_2Si_3O_{12} = CaMgSi_2O_6 + CaAl_2SiO_6 \quad (2)$$

controls the exsolution of garnet from clinopyroxene. Both reactions produce Ca-rich garnet. Reaction (1) defines a lower limit for the pressure, whereas reaction (2) defines the peak pressure of the Grt–Cpx rocks.

Clinopyroxene becomes more diopsidic [increase in Ca/(Mg + Fe) ratio] with increasing pressure because it is easier to transform the Mg- and Fe-rich pyroxene components into garnet (Akaogi & Akimoto, 1979). This leads to an increase in Ca in garnet with increasing pressure, and may be the reason for the compositional zoning observed in the garnet porphyroblasts (Fig. 8). Because of the difficulty of taking into account the effects of solid solution involving Fe^{3+} and Ti in clinopyroxene and the problem of non-stoichiometry, the exsolution of garnet, ilmenite, magnetite, and spinel (not to mention amphibole) from clinopyroxene cannot be modelled quantitatively.

Peak metamorphic temperatures for the Grt–Cpx rocks were estimated using Fe–Mg exchange data on coexisting garnet and clinopyroxene in textural equilibrium. It is well known that temperature estimates obtained from the Grt–Cpx Fe–Mg exchange thermometer are dependent on the Fe^{3+}/Fe^{2+} ratios of the two minerals. When the Fe contents in clinopyroxene are low, it is difficult to estimate the Fe^{3+}/Fe^{2+} ratios with acceptable uncertainties. Correction for Fe^{3+}/Fe^{2+} by stoichiometry and electronic charge balance often overestimates Fe^{3+}, resulting in unreasonably low

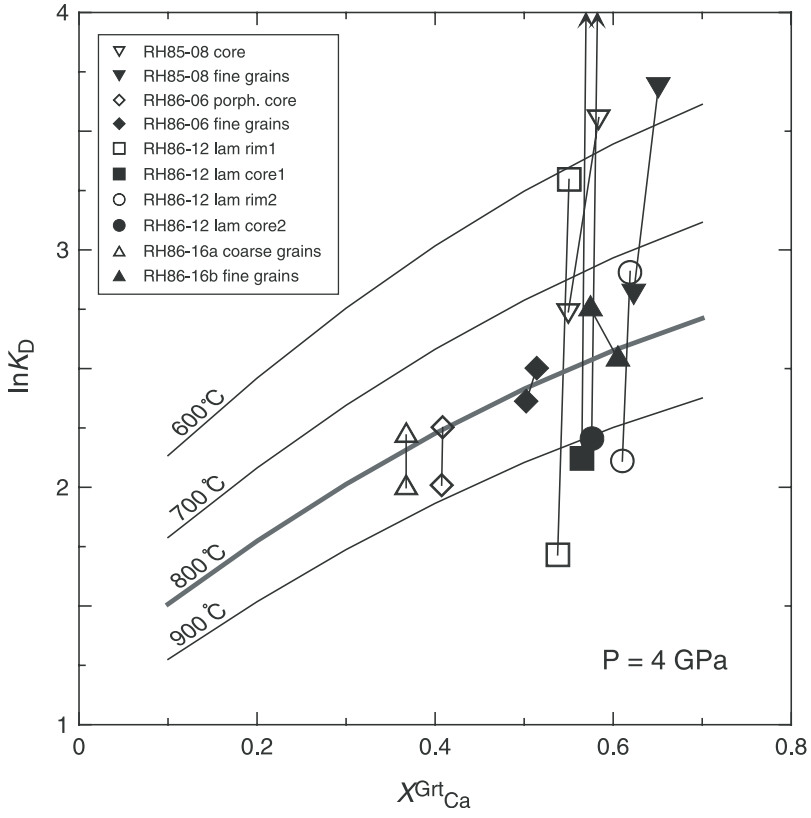

Fig. 12. ln K_D vs X^{Grt}_{Ca} (at 4 GPa) for garnet and clinopyroxene pairs. The K_D refers to the Fe–Mg exchange reaction between garnet and clinopyroxene. Isotherms are calculated using the Krogh Ravna (2000) thermometer but ignoring the dependence of K_D on Mg and Mn in garnet. Tie-lines connecting the same two symbols represent the most probable ranges of K_D for the studied Grt–Cpx pairs. porph, porphyroblast; lam, lamellar. The data used are from Tables 3 and 4.

temperature estimates. If the Fe^{2+}–Mg distribution coefficients (K_D) between garnet and clinopyroxene, with and without correction for Fe^{3+}/Fe^{2+}, are taken to be the two extreme values, a tie-line connecting the two represents the range of the most probable values of K_D. If all the studied Grt–Cpx pairs shared the same equilibrium temperature at high pressure, their K_D values must be in their corresponding ranges represented by the tie-lines. This is illustrated in a K_D vs X^{Grt}_{Ca} (where X^{Grt}_{Ca} is the mole fraction of grossular in garnet) diagram, with isotherms calculated according to the relationship calibrated by Krogh Ravna (2000) (but ignoring the dependence of K_D on Mg and Mn in garnet) (Fig. 12). At 4 GPa, one isotherm (bold line labelled 800°C) crosses the tie-lines for all the samples, except for sample RH85-08, as a result of the curvature at high X^{Grt}_{Ca}. By taking into account the temperature dependence on Mg and Mn in garnet (Krogh Ravna, 2000), the 750°C isotherm is found to lie in the ranges of K_D of all the samples. This suggests that Fe–Mg partitioning between garnet and clinopyroxene within different compositional and textural domains achieved equilibrium during high-pressure metamorphism.

The above two pressure-dependent reactions involving only the Mg end-members are calculated to constrain the peak metamorphic pressure for the Hujialin rocks by using THERMOCALC (Powell *et al.*, 1998) and the thermodynamic dataset of Holland & Powell (1998). Activities of mineral end-members are calculated as $a_{Spl} = X_{Mg}$, where $X_{Mg} = Mg/(Mg + Fe^{2+})$ in spinel; $a_{Fo} = \exp(X_{Mg}X_{Fe}W_{fofa}/RT)X^2_{Mg}$ ($W_{fofa} = 8$; R. Powell, personal communication, 2004), where $X_{Mg} = Mg/(Mg + Fe^{2+})$ and $X_{Fe} = 1 - X_{Mg}$ in olivine; $a_{Prp} = (X^X_{Mg})^3(X^Y_{Al})^2$ and $a_{Grs} = (X^X_{Ca})^3(X^Y_{Al})^2$, where $X^X_{Mg} = Mg/(Mg + Fe^{2+} + Ca + Mn)$, $X^X_{Ca} = Ca/(Mg + Fe^{2+} + Ca + Mn)$, and $X^Y_{Al} = Al/(Al + Ti + Cr + Fe^{3+})$ in garnet; $a_{CaTs} = 4X^{M1}_{Al}X^{M2}_{Ca}X^T_{Al}X^T_{Si}$ and $a_{Di} = X^{M1}_{Mg}X^{M2}_{Ca}(X^T_{Si})^2$, where $X^{M1}_{Al} = Al/(Al + Ti + Cr + Mg + Fe^{2+})$ on the M1 site, $X^{M2}_{Ca} = Ca/(Mg + Fe^{2+} + Ca + Na)$ on the M2 site, and $X^T_{Al} = Al/(Al + Si)$ and $X^T_{Si} = 1 - X^T_{Al}$ on the T sites in clinopyroxene. The results for the two reactions are given in Table 9 under 'Spl–Grt' and 'Al-in-Cpx', respectively. Intersections of the latter barometer with the Grt–Cpx Fe–Mg exchange thermometer give *P–T* estimates for four selected samples (Fig. 13). The Grt

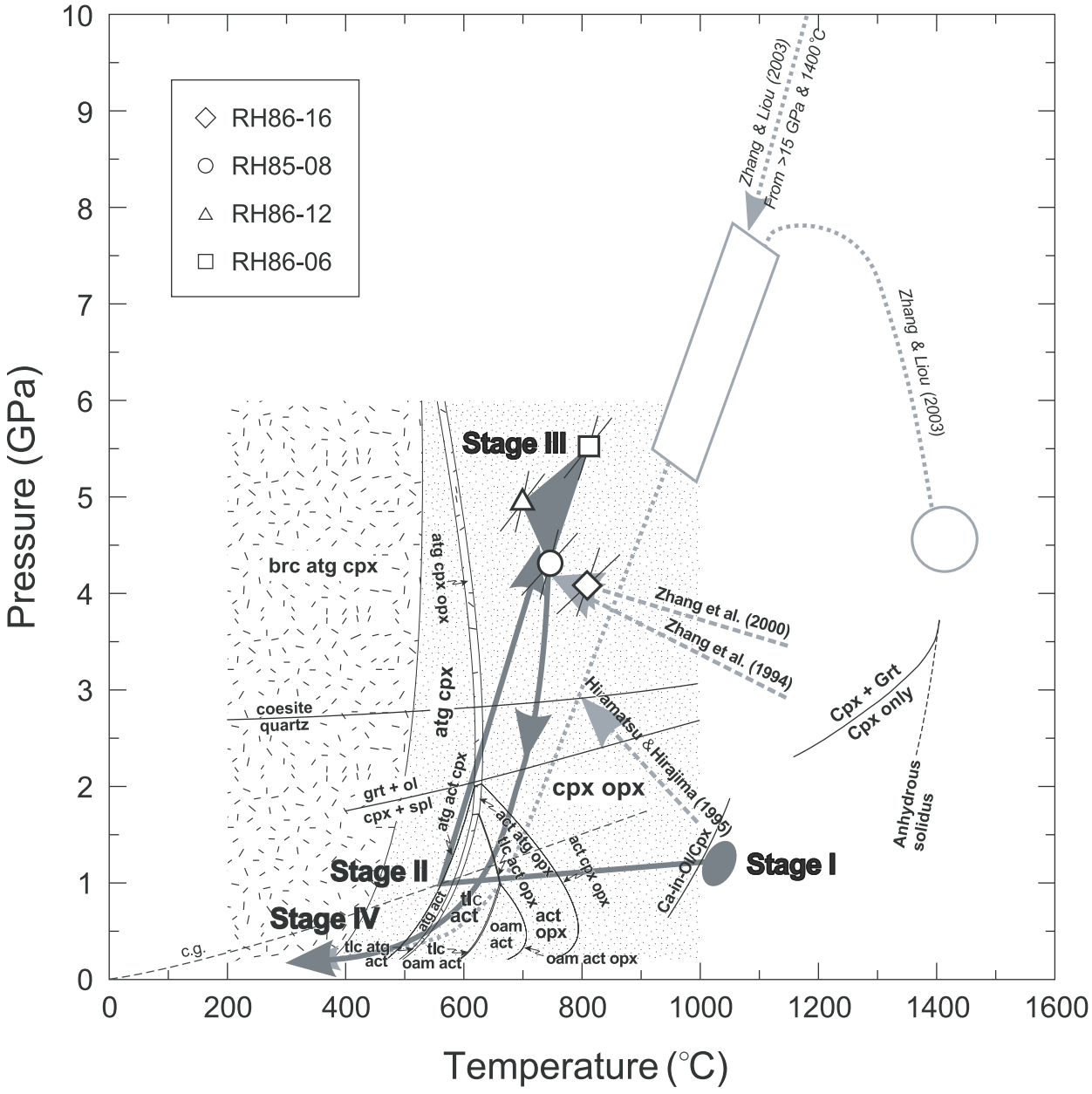

Fig. 13. *P–T* path of Hujialin Grt–Cpx rocks. Bold grey lines, this study; bold grey dashed lines, Zhang *et al.* (1994, 2000) and Hiramatsu & Hirajima (1995); bold grey dotted lines, Zhang & Liou (2003). Grey triangular area is the *P–T* estimate for peak conditions. Open box and circle are *P–T* estimates by Zhang & Liou (2003). Stage I, cumulate formation; stage II, initial cooling; stage III, UHP metamorphism; stage IV, final retrogression. Geothermobarometers used in this study: Ca-in-Ol/Cpx barometer (Köhler & Brey, 1990), calculated using the compositions of olivine inclusions and host clinopyroxene; anhydrous solidus and Cpx–Grt phase relations at high temperature are from Harte & Gurney (1975); intersecting lines: Grt–Cpx thermometer (Krogh Ravna, 2000) and Al-in-Cpx barometer; c.g., continental geotherm (England & Thompson, 1984). *P–T* pseudosection for harzburgite (SiO_2 = 37·12, CaO = 0·25, MgO = 57·33, FeO = 5·30, in mol %) in the system CaO–FeO–MgO–SiO_2–H_2O (+ ol + H_2O), the Al-in-Cpx barometer, the spl + cpx = grt + ol reaction, and the coesite = quartz transition are all calculated using THERMOCALC. Dotted areas are the trivariant fields; dashed-line areas are the divariant fields.

megacryst–Cpx inclusion pair in sample RH86-16 yields the lowest pressure. This is not surprising in view of the elastic protecting effect of the inclusion by the host. Therefore, the higher-pressure estimates for other samples, in the range of 4·2–5·4 GPa and 750 ± 50°C, may be regarded as more appropriate for the equilibrium conditions.

Given the low contents of Al in clinopyroxene, and unknown uncertainties in activity models, the uncertainties associated with the pressure estimates are

large. However, the results are similar to those of other workers in the Su–Lu terrane. The very high pressure estimates for the different Grt–Cpx rocks are consistent with the significant Na contents in garnet. Rutile needles in the coarse-grained Ca-rich garnet in sample RH86-01 may be the product of exsolution, suggesting that a minor amount of Ti was dissolved in the garnet through substitutions such as Ti + Na = Ca + Al and Ti + (Ca,Mg,Fe) = 2Al.

Harte & Gurney (1975) described granular and lamellar garnet exsolution from clinopyroxene in a Grt + Cpx inclusion in kimberlite, which has a compositional range similar to that of the Hujialin more pyrope-rich garnetite (RH86-16). The garnet in their sample contains unidentified fine acicular needles forming equilateral triangles similar to the rutile needles in the Ca-rich coarse-grained garnet from Hujialin (Fig. 4*g*). Harte & Gurney (1975) experimentally re-equilibrated a subsolidus assemblage of Cpx + Grt from 1150°C and 2·2 GPa to 1400°C and 3·8 GPa, in an anhydrous system.

Zhang & Liou (2003) proposed two hypotheses for the origin of the Hujialin Grt–Cpx rocks. The first assumed that the precursor phase was a clinopyroxenite that was crystallized at 4–5 GPa and 1400°C and was then subducted to 5–7 GPa and 900–1120°C. Their estimates for the protolith conditions were based on the experimentally determined anhydrous solidus of clinopyroxenite (Harte & Gurney, 1975), which is not directly applicable here because the Hujialin clinopyroxenite protoliths crystallized from a hydrous magma, as evidenced by the presence of amphibole inclusions and lamellae in clinopyroxene. Their second hypothesis assumed that the precursor mineral was a majoritic garnet formed at 15 GPa and 1500°C, from which clinopyroxene exsolved as a result of cooling and decompression. There is, however, no evidence for the existence of majoritic garnet in the Hujialin rocks. On the contrary, the TiO_2 content of the Hujialin garnet is $\leq$0·48 wt %, far below the range (0·8–4·5 wt %) of garnet synthesized at 5–15 GPa in their experiments (Zhang *et al.*, 2003). Moreover, the REE patterns of clinopyroxene are not similar to those of garnet (Fig. 7a), and, thus, not in favour of an exsolution origin from garnet.

As relatively fast cooling from the igneous stage prohibits extensive exsolution from taking place, it is suggested that the clinopyroxenite protoliths at Hujialin first cooled to a low temperature with only minor or no garnet exsolution; more extensive exsolution of garnet took place during subsequent subduction metamorphism. Implicit with the negatively sloping *P–T* paths proposed by Zhang *et al.* (1994, 2000) and Hiramatsu & Hirajima (1995) is an assumption that the cumulates cooled while subducting to great depth. This interpretation is not supported by the existing data. The high-temperature condition of crystallization for the cumulates is not typical of the surrounding mantle rocks, and it is more reasonable to envisage that the cumulates cooled to a temperature concordant with a normal geotherm appropriate for the crust–mantle boundary after their emplacement (Fig. 13).

After peak metamorphism, the Hujialin rocks experienced amphibolite-facies metamorphism, as recorded by amphibole and chlorite in the matrix and titanite + zoisite after garnet. The minor, inhomogeneous, and variably Ca- and Mn-enriched garnet rims and their frequently sharp contacts with the cores (Fig. 4f) suggest that they are unlikely to be representative of the equilibrium composition of the garnet at the peak metamorphic stage, but rather resulted from late-stage Ca enrichment by fluids from the coevally serpentinizing host ultramafic rock.

No sign of the UHP metamorphic history is preserved in the serpentinites and harzburgite at and near Hujialin (Fig. 1), except for the occurrence of layers of UHP eclogites and Grt–Cpx rocks in them. In the harzburgite, orthopyroxene and actinolite occur both as rare porphyroblasts and in the matrix, and talc and olivine crystallized at the expense of orthopyroxene. These indicate a retrograde part of the *P–T* path, as shown by a pseudosection in the system CaO–FeO–MgO–SiO_2–H_2O, with olivine and H_2O in excess (Fig. 13). Based on these considerations and the *P–T* estimates made above, the *P–T* path inferred for the Hujialin Grt–Cpx rocks, shared by the enclosing ultramafic rocks, is outlined in Fig. 13. The *P–T* paths proposed by previous workers are also shown for comparison.

CONCLUSIONS

(1) The Hujialin Ca-rich Grt–Cpx layers in host ultramafic rocks were derived from spinel clinopyroxenites by exsolution of Ca-rich garnet, magnetite, ilmenite and hercynite from augite and transformation of spinel into garnet, as a result of burial. They were subjected to minor Ca enrichment coeval with serpentinization of the host ultramafic rocks after exhumation. The Grt–Cpx rocks cannot be the protolith of the Su–Lu garnet peridotites, nor are they slices of mantle pyroxenite, as proposed elsewhere.

(2) The reconstructed compositions [Al_2O_3 vs Mg/(Mg + Fe^{2+}) correlation, Al^{IV}/Ti ratios, Ca–Mg–Fe proportions and high Fe^{3+} contents] of the original igneous augite, the presence of pargasite inclusions in clinopyroxene, and isotope compositions suggest that the Hujialin clinopyroxenites crystallized from a hydrous, subduction-related, magma beneath an arc. Their relatively low Mg/(Mg + Fe), Cr and Ni, and high Al, Ti, Zr, and V contents suggest that they were cumulates not from

primary magmas in equilibrium with the mantle, but from magmas that had differentiated to variable extents.

(3) Peak metamorphic conditions for the Hujialin Grt–Cpx rocks are estimated to be in the range 4·8 ± 0·6 GPa and 750 ± 50°C. The lack of evidence for the former existence of a majorite component, and the low TiO_2 content in garnet, precludes the possibility that the rocks re-equilibrated at pressures >6 GPa. The minor rutile needles in coarse-grained Ca-rich garnet in sample RH86-01 imply only minor amounts of Ti + Na = Al + Ca and/or Ti + (Ca,Mg,Fe) = 2Al substitutions in such garnet, if they were indeed the products of exsolution from the garnet.

(4) Given that cooling to the temperature of the surrounding lithosphere seems unavoidable after the igneous stage, the negatively sloped *P–T* paths proposed by some earlier workers for the Hujialin Grt–Cpx rocks are questionable. In any case, such *P–T* paths should not be used to argue for corner flow and mantle wedge subduction, because the Hujialin spinel clinopyroxenites probably crystallized in the lithosphere near the crust–mantle boundary, rather than in the asthenospheric mantle.

ACKNOWLEDGEMENTS

L. Liu and H.-L. Yuan helped with ICP-MS analysis, Q. Mao and Y.-G. Ma with electron microprobe analysis. Advice from R. Powell on calculating pseudo-sections, and discussion with the late Dr. S.-s. Sun, X.-P. Li and W. Lin are much appreciated. J. Hermann, T. H. Green, G. Clarke and M. Wilson provided helpful reviews and editorial comments, which considerably improved the manuscript. This work was supported by the Natural Science Foundation of China (Nos 40473022 and 40421202) and the Chinese Academy of Sciences (KZCX3-SW-135).

REFERENCES

Akaogi, M. & Akimoto, S. (1979). High-pressure phase equilibria in a garnet lherzolite, with special reference to Mg^{2+}–Fe^{2+} partitioning among constituent minerals. *Physics of the Earth and Planetary Interiors* **19**, 31–51.

Anders, E. & Grevesse, N. (1989). Abundances of the elements: meteoritic and solar. *Geochimica et Cosmochimica Acta* **53**, 197–214.

Becker, H. (1996). Crustal trace element and isotopic signatures in garnet pyroxenites from garnet peridotite massifs from lower Austria. *Journal of Petrology* **37**, 785–810.

Becker, H. & Altherr, R. (1992). Evidence from ultra-high-pressure marbles for recycling of sediments into the mantle. *Nature* **358**, 745–748.

Chen, J., Xu, Z., Li, X., Chen, Z., Li, T. & Chen, F. (2003). Exsolution textures of pargasites and ilmenites in clinopyroxenes of garnet pyroxenite from the Sulu UHP terrane and their geological implications. *Acta Geologica Sinica* **77**, 556–565.

Conrad, W. K. & Kay, R. W. (1984). Ultramafic and mafic inclusions from Akak Island: crystallization history, and implications for the nature of primary magmas and crustal evolution in the Aleutian Arc. *Journal of Petrology* **25**, 88–125.

Debari, S. M. & Coleman, R. G. (1989). Examination of the deep levels of an island arc: evidence from the Tonsina ultramafic–mafic assemblage, Tonsina, Alaska. *Journal of Geophysical Research* **94**, 4373–4391.

Debari, S. M. & Coleman, R. G. (1991). High-Mg, low-Al bulk composition of the Talkeetna island arc, Alaska: implications for primary magmas and the nature of arc crust. *Geological Society of America Bulletin* **103**, 37–46.

Dick, H. J. B. & Bullen, T. (1984). Chromium spinel as a petrogenetic indicator in abyssal and Alpine-type peridotites and spatially associated lavas. *Contributions to Mineralogy and Petrology* **86**, 54–76.

Droop, G. T. R. (1987). A general equation for estimating Fe^{3+} concentrations in ferromagnesian silicates and oxides from microprobe analyses, using stoichiometric criteria. *Mineralogical Magazine* **51**, 431–435.

England, P. C. & Thompson, A. B. (1984). Pressure–temperature–time paths of regional metamorphism, Part I: Heat transfer during the evolution of regions of thickened continental crust. *Journal of Petrology* **25**, 894–928.

Evans, B. W., Trommsdorff, V. & Richter, W. (1979). Petrology of an eclogite–metarodingite suite at Cima di Gagnone, Ticino, Switzerland. *American Mineralogist* **64**, 15–31.

Gao, S., Liu, X., Yuan, H., Hattendorf, B., Günther, D., Chen, L. & Hu, S. (2002). Analysis of forty-two major and trace elements of USGS and NIST SRM glasses by LA-ICPMS. *Geostandards Newsletter* **26**, 181–196.

Gao, T., Chen, J., Xie, Z., Yang, S. & Yu, G. (2004). Zircon SHRIMP U–Pb age of garnet olivine pyroxenite at Hujialin in the Sulu terrane and its geological significance. *Chinese Science Bulletin* **49**, 2198–2204.

Gust, D. A. & Perfit, M. R. (1987). Phase relations of a high-Mg basalt from the Aleutian island arc: implications for primary island arc basalts and high-Al basalts. *Contributions to Mineralogy and Petrology* **97**, 7–18.

Hacker, B. R., Ratschbacher, L., Webb, L., Ireland, T., Walker, D. & Shuwen, D. (1998). U/Pb zircon ages constrain the architecture of the ultrahigh-pressure Qinling–Dabie Orogen, China. *Earth and Planetary Science Letters* **161**, 215–230.

Harte, B. & Gurney, J. J. (1975). Evolution of clinopyroxene and garnet in an eclogite nodule from the Roberts Victor kimberlite pipe, South Africa. *Physics and Chemistry of the Earth* **9**, 367–387.

Hauri, E. H., Gaetani, G. & Green, T. H. (2004). Partitioning of H_2O between mantle minerals and silicate melts. *Geochimica et Cosmochimica Acta* **68**, A33.

Hiramatsu, N. & Hirajima, T. (1995). Petrology of the Hujialin garnet clinopyroxenite in the Su–Lu ultrahigh-pressure province, eastern China. *The Island Arc* **4**, 310–323.

Hofmann, A. W. (1988). Chemical differentiation of the Earth: the relationship between mantle, continental crust, and oceanic crust. *Earth and Planetary Science Letters* **90**, 297–314.

Holland, T. J. B. & Powell, R. (1998). An internally consistent thermodynamic dataset for phases of petrological interest. *Journal of Metamorphic Geology* **16**, 309–343.

Holm, P. M. (2002). Sr, Nd and Pb isotopic composition of *in situ* lower crust at the Southwest Indian Ridge: results from ODP Leg 176. *Chemical Geology* **184**, 195–216.

Jahn, B.-M. (1999). Sm–Nd isotope tracer study of UHP metamorphic rocks: implications for continental subduction and collisional tectonics. *International Geology Review* **41**, 859–885.

Jerde, E. A., Taylor, L. A., Crozaz, G. & Sobolev, N. V. (1993). Exsolution of garnet within clinopyroxene of mantle eclogites: major and trace element chemistry. *Contributions to Mineralogy and Petrology* **114**, 148–159.

Klemd, R., Matthes, S. & Schüssler, U. (1994). Reaction textures and fluid behaviour in very high-pressure calc-silicate rocks of the Münchberg gneiss complex, Bavaria, Germany. *Journal of Metamorphic Geology* **12**, 735–745.

Koepke, J., Seidel, E. & Kreuzer, H. (2002). Ophiolites on the Southern Aegean islands Crete, Karpathos and Rhodes: composition, geochronology and position within the ophiolite belts of the Eastern Mediterranean. *Lithos* **65**, 183–203.

Köhler, T. P. & Brey, G. (1990). Calcium exchange between olivine and clinopyroxene calibrated as a geothermobarometer for natural peridotites from 2 to 60 kb with applications. *Geochimica et Cosmochimica Acta* **54**, 2375–2388.

Kretz, R. (1983). Symbols for rock forming minerals. *American Mineralogist* **68**, 277–279.

Krogh Ravna, E. J. (2000). The garnet–clinopyroxene Fe^{2+}–Mg geothermometer: an updated calibration. *Journal of Metamorphic Geology* **18**, 211–219.

Li, S. (1993). Collision of the North China and Yangtze blocks and formation of coesite-bearing eclogites: timing and processes. *Chemical Geology* **109**, 89–111.

Liu, F., Xu, Z., Liou, J. G. & Song, B. (2004). SHRIMP U–Pb ages of ultrahigh-pressure and retrograde metamorphism of gneisses, south-western Sulu terrane, eastern China. *Journal of Metamorphic Geology* **22**, 315–326.

Loucks, R. R. (1990). Discrimination of ophiolitic from nonophiolitic ultramafic–mafic allochthons in orogenic belts by the Al/Ti ratio in clinopyroxene. *Geology* **18**, 346–349.

Melcher, F., Meisel, T., Puhl, J. & Koller, F. (2002). Petrogenesis and geotectonic setting of ultramafic rocks in the Eastern Alps: constraints from geochemistry. *Lithos* **65**, 69–112.

Miyashiro, A. & Shido, F. (1975). Tholeiitic and calc-alkalic series in relation to the behaviours of titanium, vanadium, chromium, and nickel. *American Journal of Science* **275**, 265–277.

Müntener, O., Kelemen, P. B. & Grove, T. L. (2001). The role of H_2O during crystallization of primitive arc magmas under uppermost mantle conditions and genesis of igneous pyroxenites: an experimental study. *Contributions to Mineralogy and Petrology* **141**, 643–658.

O'Hara, M. J. & Mercy, E. L. P. (1966). Exceptionally calcic pyralspite from South African kyanite eclogite. *Nature* **212**, 68–69.

Parlak, O., Hock, V. & Delaloye, M. (2002). The supra-subduction zone Pozanti–Karsanti ophiolite, southern Turkey: evidence for high-pressure crystal fractionation of ultramafic cumulates. *Lithos* **65**, 205–224.

Powell, R., Holland, T. J. B. & Worley, B. (1998). Calculating phase diagrams involving solid solutions via non-linear equations, with examples using THERMOCALC. *Journal of Metamorphic Geology* **16**, 577–588.

Rösli, U., Hoernes, S. & Koppel, V. (1991). Isotope data of metarodingites and associated rocks from the Lanzo and the Bracco ophiolitic massifs: indications on the evolution of the Alpine-type ultramafic–mafic complexes. *Schweizerische Mineralogische und Petrographische Mitteilungen* **71**, 125–141.

Scambelluri, M. & Rampone, E. (1999). Mg-metasomatism of oceanic gabbros and its control on Ti-clinohumite formation during eclogitization. *Contributions to Mineralogy and Petrology* **135**, 1–17.

Scharbert, H. G. & Carswell, D. A. (1983). Petrology of garnet–clinopyroxene rocks in a granulite facies environment, Bohemian massif of Lower Austria. *Bulletin de Minéralogie* **106**, 761–774.

Suen, C. J. & Frey, F. A. (1987). Origins of the mafic and ultramafic rocks in the Ronda peridotite. *Earth and Planetary Science Letters* **85**, 183–202.

Vrána, S. & Frýda, J. (2003). Ultrahigh-pressure grossular-rich garnetite from the Moldanubian Zone, Czech Republic. *European Journal of Mineralogy* **15**, 43–54.

Yang, J.-J. (1991). *Eclogites, Garnet Pyroxenites, and Related Ultramafics in Shandong and North Jiangsu of East China*. Beijing: Geological Publishing House.

Yang, J.-J. (1992). A new scheme for calculating mineral end-members with reference to garnet and clinopyroxene. *Acta Geologica Sinica* **5**, 191–196.

Yang, J.-J. (2003). Relict edenite in a garnet lherzolite from the Chinese Su–Lu UHP metamorphic terrane: implications for metamorphic history. *American Mineralogist* **88**, 180–188.

Yang, J.-J. & Jahn, B.-M. (2000). Deep subduction of mantle-derived garnet peridotites from the Su–Lu UHP metamorphic terrane in China. *Journal of Metamorphic Geology* **18**, 167–180.

Yang, J.-J. & Smith, D. C. (1989). Evidence for a former sanidine coesite eclogite at Lanshantou, eastern China, and the recognition of the Chinese 'Su–Lu Coesite–Eclogite-Province'. *Terra Abstracts* **1**, 26.

Yang, T.-N., Zeng, L. S. & Liou, J. G. (2005). Mineral evolution of a garnet-pyroxenite nodule within eclogite, eastern Sulu ultrahigh pressure metamorphic terrane, East China. *Journal of Metamorphic Geology* **23**, 667–680.

Zhang, R. Y. & Liou, J. G. (2003). Clinopyroxenite from the Sulu ultrahigh-pressure terrane, eastern China: origin and evolution of garnet exsolution in clinopyroxene. *American Mineralogist* **88**, 1591–1600.

Zhang, R. Y., Liou, J. G. & Cong, B. L. (1994). Petrogenesis of garnet-bearing ultramafic rocks and associated eclogites in the Su–Lu ultrahigh-*P* metamorphic terrane, eastern China. *Journal of Metamorphic Geology* **12**, 169–186.

Zhang, R. Y., Liou, J. G., Yang, J. S. & Yui, T.-F. (2000). Petrochemical constraints for dual origin of garnet peridotites from the Dabie–Sulu UHP terrane, eastern–central China. *Journal of Metamorphic Geology* **18**, 149–166.

Zhang, R. Y., Zhai, S. M., Fei, Y. W. & Liou, J. G. (2003). Titanium solubility in coexisting garnet and clinopyroxene at very high pressure: the significance of exsolved rutile in garnet. *Earth and Planetary Science Letters* **216**, 591–601.